Sharpened and mechanically robust carbon fiber electrode arrays for neural interfacing

Elissa J Welle[1,2], Joshua E Woods[3], Ahmad A. Jiman[1,2,4], Julianna M Richie[1,2], Elizabeth C Bottorff[1,2], Zhonghua Ouyang[1,2], John P Seymour[1,3,5], Paras R Patel[1,2], Tim M Bruns[1,2], Cynthia A Chestek[1,2,3,6,7]

1. Department of Biomedical Engineering, University of Michigan, Ann Arbor, MI
2. Biointerfaces Institute, University of Michigan, Ann Arbor, MI
3. Department of Electrical Engineering and Computer Science, University of Michigan, Ann Arbor, MI
4. Department of Electrical and Computer Engineering, King Abdulaziz University, Jeddah, Saudi Arabia
5. Department of Neurosurgery, University of Texas Health Science Center, Houston, TX
6. Neuroscience Graduate Program, University of Michigan, Ann Arbor, MI
7. Robotics Graduate Program, University of Michigan, Ann Arbor, MI

Abstract

Objective: Bioelectric medicine offers therapeutic diagnoses and treatments for disorders of the nervous system unresponsive to pharmacological treatments. While current neural interfaces effectively treat many disorders with stimulation, recording specificity is often limited to gross averages across many neurons or axons. Here, we develop and describe a novel, robust carbon fiber electrode array adaptable to many neural structures for precise neural recording. *Approach:* Carbon fibers were sharpened using a blowtorch method made reproducible by using the reflection of fibers against the surface of a water bath. Arrays of carbon fibers were developed by partially embedding carbon fibers in medical-grade silicone to improve robustness to fracture. Acute spontaneous electrophysiology was recorded from the rat cervical vagus nerve, feline dorsal root ganglia, and rat brain. Acute brushing and bladder pressure electrophysiology was recorded from feline dorsal root ganglia as well. *Main results:* Blowtorching resulted in fibers of 72.3 ± 33.5 degree tip angle with 146.8 ± 17.7 µm exposed carbon. Silicone-embedded carbon fiber arrays were robust to bending (87.5% of fibers remained unbroken, 50,000 passes). Observable neural clusters were recorded using sharpened carbon fiber electrodes from rat cervical vagus nerve (41.8 μV_{pp}, N=3 electrodes), feline dorsal root ganglia (101.1 μV_{pp}, N=32 electrodes), and rat brain (80.7 μV_{pp}, N=7 electrodes). Recordings from the feline dorsal root ganglia included physiologically-relevant signals from increased bladder pressure and cutaneous brushing. *Significance:* These results suggest that this carbon fiber array is a uniquely robust and adaptable neural recording device, useful for specific electrophysiology measurements. In the future, this device may be useful as a bioelectric medicine tool for diagnosis and closed-loop neural control of therapeutic treatments and monitoring systems.

Keywords: carbon fiber, electrophysiology, neural electrode, peripheral nerve interfacing, dorsal root ganglia, motor cortex, vagus nerve

Introduction

Bioelectric medicine is the branch of therapeutic modalities that use electrical stimulation to treat disorders of the nervous system (Birmingham et al., 2014). Recent applications include vagus nerve stimulation for inflammation (Andersson & Tracey, 2012) and therapy-resistant depression (Müller et al., 2018). These novel developments build upon well-established uses such as sacral nerve stimulation for bladder diseases (Schmidt et al., 1999), vagus nerve stimulation for epilepsy (DeGiorgio et al., 2005), and deep brain stimulation for Parkinson's disease (Deuschl et al., 2006). Devices in bioelectric medicine incorporate unique electrode configurations, materials, stimulation patterns, and closed-loop control to precisely modulate target organs functions (Famm, Litt, Tracey, Boyden, & Slaoui, 2013; Horn, Ardell, & Fisher, 2019).

Current electrode interfaces for neural stimulation are large extraneural leads (Janssen, Martens, de Wall, van Breda, & Heesakkers, 2017; Siegel et al., 2018) or nerve cuffs (Charkhkar, Christie, Pinault, Tyler, & Triolo, 2019; Navarro et al., 2005). While these interfaces have shown efficacy, they have limited selectivity and can lead to side effects (Panebianco, Rigby, Weston, & Marson, 2015). Furthermore,

these interfaces have minimal utility for monitoring neural signals to examine the mechanisms of organ control or to obtain organ-state signals for closed-loop control that may improve the efficacy of current open-loop bioelectric medicine therapies.

Intraneural interfaces, such as the Utah Slanted Electrode Array (USEA) (Branner, Stein, & Normann, 2001; Wark et al., 2013) and the longitudinal and transverse intrafascicular electrode array (Badia et al., 2011; Boretius et al., 2010; Lago, Yoshida, Koch, & Navarro, 2007; Yoshida, Hennings, & Kammer, 2006), offer greater recording signal-to-noise ratio and stimulation selectivity (Larson & Meng, 2020; Patil & Thakor, 2016). The selective access to axons and fascicles enabled by conventional intraneural interfaces has facilitated clinical research of nerve-machine interfaces (del Valle & Navarro, 2013). Nerve-machine interfaces connect peripheral nerves to an external robotic device, allowing the nervous system to send motor commands to (Micera et al., 2011; Page et al., 2018), and receive sensory input from the device (Davis et al., 2016; Tan et al., 2014). However current interfaces have limited long-term viability due to electrode material failure (Grill, Norman, & Bellamkonda, 2009; Straka, Shafer, Vasudevan, Welle, & Rieth, 2018; Takmakov et al., 2015) and significant scarring (Branner, Stein, Fernandez, Aoyagi, & Normann, 2004; Christensen et al., 2014; Kolarcik et al., 2020; Wark, Mathews, Normann, & Fernandez, 2014). Additionally, their size is not appropriate for the small nerves of the autonomic nervous system, which provide primary innervation of organs. An ideal interface with autonomic nerves would maximize recording specificity while minimizing scarring, maintain a high channel count of small-footprint electrodes, and contain robust, biocompatible electrode materials.

Some recent interface designs are beginning to come close to these criteria. Novel electrode development often starts with cortical applications that may later undergo translation to more peripheral target locations. An injectable mesh-style PDMS array with 10 µm-diameter elements prompted minimal histological scarring and maintained long-term recording in the brain (Hong et al., 2018; Liu et al., 2015). However, the injection method of insertion would make this difficult to use in peripheral applications. Flexible carbon nanotube "yarn" electrodes recently demonstrated physiologically-relevant recordings in the rat cervical vagus and glossopharyngeal nerves for up to 16 weeks with minimal scarring (McCallum et al., 2017). This suggests that ultra-small electrodes may be similarly biocompatible with nerves, as has been shown in the brain (Kozai et al., 2012; Patel et al., 2016; Seymour & Kipke, 2007; Skousen et al., 2011). While capable of recording from awake and behaving animals, this electrode design is limited by the fragile structure of the carbon nanotube material and the manual insertion of each electrode with a shuttle or suture, which may limit channel count (Marmerstein, McCallum, & Durand, 2021).

Neural interfaces constructed of rigid components at micron size scale may ease surgical implementation while still minimizing tissue response. Recently, a 3-D printed clip interface demonstrated chronic stimulation and recording of small diameter rat nerves (Otchy et al., 2020). Although adaptable to individual nerve sizes and less surgically intensive in its implantation, this design still utilizes extraneural recordings, which may reduce spatial selectivity. Another novel design uses carbon fiber electrodes, which have been primarily used for brain recordings (Guitchounts, Markowitz, Liberti, & Gardner, 2013; Patel et al., 2015; Welle et al., 2020), as a method to record from nerves (Gillis et al., 2017). The carbon fiber electrodes reported in Gillis et al., 2017 successfully recorded spontaneous spiking activity, but the majority of their recordings were evoked responses to electrical stimulation. Additionally, the architecture of their array would be difficult to translate from acute experimentation to chronic implantation, and the carbon fiber electrodes' rigid junction to the substrate provides a likely breakage point. An array with sub-cellular carbon fiber electrodes that is compatible with peripheral geometry and capable of spontaneous neural recording is needed for neural interfacing.

Here, we develop and demonstrate a carbon fiber array comprised of several novel components: sharpened carbon fibers ranging from 200–1100 µm length for insertion into neural structures of varying dimensions, embedded carbon fibers in a silicone body for enhanced robustness and strain relief, and a small (< 2 mm in any dimension) overall device architecture. We test the unique components of the array in the rat cervical vagus nerve, feline dorsal root ganglion, and rat motor cortex. Our *in vivo* tests of sharpened carbon fibers show insertion into neural structures of varying stiffness and to various depths. We demonstrate that sharpened carbon fiber arrays record both spontaneous and physiologically-relevant neural clusters. Additionally, we verify that the small device architecture still enables surgical handling while accessing neural structures of differing geometries. Our benchtop experiments test the robustness of the carbon fibers embedded in silicone and the capability to survive many repeated cycles of bending. This work showcases a versatile, unique set of capabilities for carbon fiber arrays in neural interfacing.

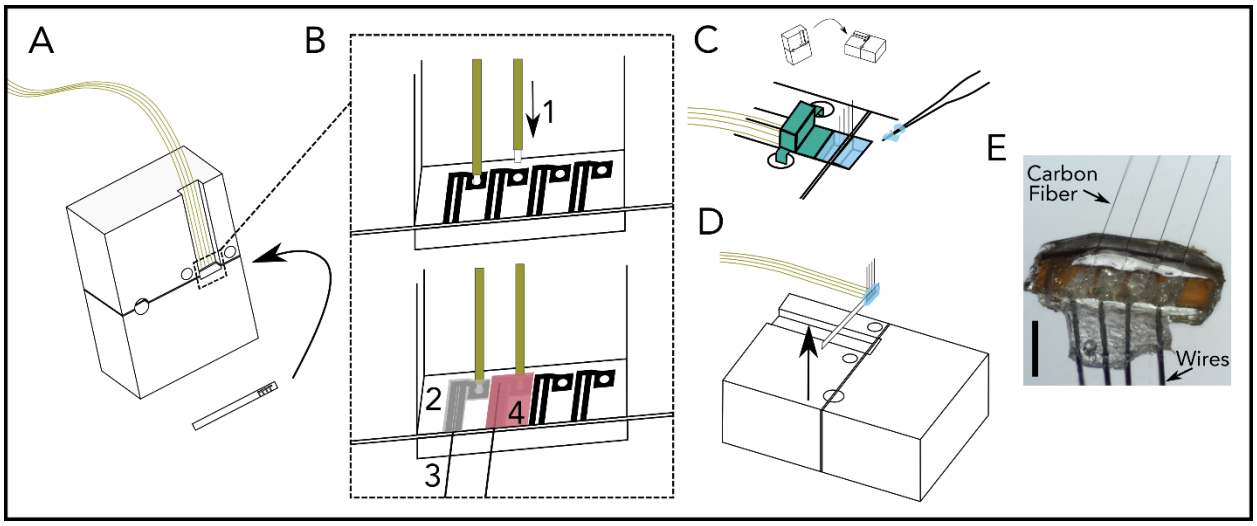

Figure 1. Carbon fiber silicone array (CFSA) fabrication schematic. A) A custom polyimide printed circuit board is slotted into a custom aluminum holder and four polyimide-insulated wires are secured to the aluminum mold above the area of interest on the polyimide board. B) The wires and carbon fibers are electrically connected and secured to the polyimide board. B1) The tip of each wire is exposed from polyimide insulation and placed into the gold-plated vias in the polyimide printed circuit board. B2) Silver epoxy is applied to the pair of connected gold traces and the adjoining gold-plated via. B3) Bare carbon fibers are placed in the silver epoxy between the pair of gold traces and the epoxy is then cured. B4) Insulating epoxy is applied over the electrical connections, and then cured. C) The aluminum holder is laid down flat and a 3-D printed device is placed over the wires to create a well for the silicone. The silicone is applied with pulled glass capillaries and then cured. D) The 3-D printed wall is removed and the polyimide board with attached wires, carbon fibers, and silicone is lifted from the aluminum mold. E) A picture of the CFSA with the excess tails of polyimide board on either side of the silicone removed. Scale bar is 500 µm.

Methods

1.1 Fabrication of Carbon Fiber Flex Array

Acute neural recordings from the rat cervical vagus nerve (CVN) and feline dorsal root ganglia (DRG) were collected using carbon fiber electrode arrays previously detailed in Patel et al., 2020. The electrode array, termed Flex Array, features a 100 µm-thick custom polyimide printed circuit board (PCB) body with a long, flexible shaft designed to access deep brain structures via a glass cannula. Full fabrication steps for Flex Arrays are found in Patel et al. 2020 and are briefly summarized here. A 32-channel connector (A79024-001, Omnetics, Minneapolis, MN, USA) was soldered to the bond pads at one end of the polyimide PCB (MicroConnex, Snoqualmie, WA, USA) and reinforced with 2-part quick-curing epoxy. The other end of the polyimide PCB was populated with up to 16 individuated carbon fibers spaced 132 µm apart. The uninsulated carbon fibers (6.8 µm diameter) (T-650/35 3K, Cytec Thornel, Woodland Park, NJ, USA) were attached to gold bond pads with conductive silver epoxy (H20E, Epoxy Technology, Inc., Billerica, MA, USA). After baking, the traces were insulated with UV-curable epoxy (OG142-87, Epoxy Technology, Inc., Billerica, MA, USA). The device was coated with approximately 800 nm of parylene-c (PDS2035CR, Specialty Coatings Systems, Indianapolis, IN, USA). After coating, the carbon fibers were cut to lengths between 150 µm to 200 µm, based on intended tip preparation method, using stainless steel microsurgical scissors (15002-08, Fine Science Tools, Foster City, CA, USA) under a stereoscope equipped with a reticle.

1.2 Fabrication of Carbon Fiber Silicone Array (CFSA)

This study exhibits a novel carbon fiber silicone array (CFSA) featuring carbon fiber electrodes partially embedded in silicone and attached to a connector with wires and an interface PCB. The fabrication process is depicted in Figure 1. The foundation of the array is a custom polyimide PCB (MicroConnex, Snoqualmie, WA, USA), 450 µm x 6.81 mm x 50 µm in size (length x width x thickness). The CFSA is built on a 1.5 mm long exposed section of the PCB in which 4 pairs of 65 µm pitch, 430 µm-long gold traces are positioned 310 µm apart (Figure 1B). Each trace pair is connected to a 90 µm-diameter gold-plated via. During fabrication, the polyimide PCB is slotted into a custom aluminum holder (Figure 1A) (Protolabs, Maple Plain, MN, USA) and secured with double-sided carbon tape (16086-8, Ted Pella, Inc., Redding, CA, USA). A thin piece of carbon tape is attached to the bottom of a 1.75 mm x 0.60 mm depression in the aluminum holder perpendicular to the exposed gold traces.

A custom interface PCB was designed to interface with either a 32 or 16-channel Omnetics connector (A79024-001 or A79040-001, Omnetics, Minneapolis, MN, USA) and four 10 cm-long wires (50.8 µm diameter 35N LT, coated with

polyimide to 60.9 µm) (Fort Wayne Metals, Fort Wayne, IN, USA). One end of the wires were exposed by removing roughly 5 mm of polyimide insulation with hot tweezers (HOTweezers, Rustington, West Sussex, United Kingdom). The connector and four wires were soldered to the interface PCB and secured with 2-part quick curing epoxy. The other end of the wires were similarly exposed by removing 75 µm of polyimide insulation.

Next, the interface PCB and aluminum holder containing the polyimide PCB were aligned roughly 5 cm apart and the aluminum holder was tilted to roughly 30 degrees to accommodate the natural arch of the wires. The 75 µm uninsulated tip of each wire was slotted into a gold-plated via in the polyimide PCB while the proximal section of insulated wire was secured to the carbon tape in the aluminum holder depression to prevent detachment (Figure 1B-1).

Silver epoxy (H20E, Epoxy Technology, Inc., Billerica, MA, USA) was applied to the junction of the wire at the via and the adjoining pair of gold traces with a pulled glass capillary, similar to the Flex Array (Figure 1B-2). Individual carbon fibers of roughly 3 mm length were placed in the silver epoxy between the paired gold traces until fully submerged and parallel with the traces (Figure 1B-3). The epoxy was then cured with the manufacturer's recommended settings. A layer of insulating epoxy (353ND- T, Epoxy Technology, Inc., Billerica, MA, USA) was applied over traces and wire junctions, and cured with the manufacturer's recommended settings (Figure 1B-4).

A custom 3D-printed piece was situated in the depression of the aluminum holder over the wires to create a well around the CFSA for the silicone molding (Figure 1C). Pulled glass capillaries shuttled the degassed medical grade silicone (A-103, Factor II, Lakeside, AZ, USA) into the 200 µm-wide areas on either side of the polyimide PCB. Once silicone reached the height of the polyimide PCB, small droplets of silicone were applied between the fibers to bridge the two sides of silicone above the polyimide PCB. The aluminum holder was then moved to a hotplate and the silicone was cured at 110° C for 20 minutes.

The 3D printed wall was removed and the entire device was coated with approximately 800 nm of parylene-c. The polyimide PCB embedded in silicone with attached wires was removed from the aluminum holder by gently pulling on the free end of the PCB with forceps (Figure 1D). Once removed, the carbon fibers were trimmed to length (500-1100 µm based on application) with microsurgical scissors prior to electrode tip processing (Figure 1E).

1.3 Sharpening of Carbon Fiber Electrode Tip

We adapted a heat-based sharpening method using a butane torch to our carbon fiber arrays. Building upon previous demonstrations of torched carbon fibers in long fiber bundles (Guitchounts et al., 2013), or relatively long, individuated fibers (Gillis et al., 2017), we advanced this technique to work with short fibers suitable for dwelling within 300–500 µm-diameter nerves. Our method uses the reflective properties of water to precisely align short fibers for sharpening, while keeping the body of the array safely away from the flame under the water's surface (Figure 2).

Both carbon fiber array types, Flex Arrays and CFSAs, underwent a similar sharpening procedure but were held using different mechanisms. Given the large size of the Flex Array, the connector end of the Flex Array was secured with putty to the base of a glass dish whose walls were taller than the length of the array (Figure 2A). Water was added to the dish until the array was completely submerged. The water level was adjusted using a pipette. The small, lightweight nature of the CFSAs required that the array be held by nerve forceps (ASSI.NHF0.5, Accurate Surgical & Scientific Instruments Corp., Westbury, NY, USA) and lowered into the water (Figure 2B). The nerve forceps clamped the free end of the polyimide PCB of the CFSA at a 45 degree angle. The forceps were secured to a stereotaxic frame angled such that the CFSA was parallel to the water surface with carbon fibers pointing up. The CFSA was then manually lowered into a dish of water until fibers were submerged. Once an array was submerged, an endoscopic camera (MS100, Teslong, Shenzhen, China) was aligned outside the glass dish and focused on the reflection of the fibers on the underside of the water surface. The height of the carbon fibers was adjusted relative to the water height until the true fiber image touched the fiber reflection on the underside of the water surface (Figure 2A, B insets). A microtorch (MT-51B, Master Appliance, Racine, WI, USA) with an approximately 3 mm diameter butane flame was then passed over the fibers, sharpening them to a point to create sharpened carbon fibers (SCFs) (Figure 2C). Sharpening was confirmed by visual inspection under a microscope. Multiple passes of the microtorch were occasionally necessary to sharpen all fibers on an array.

1.4 Scanning Electron Microscopy (SEM) Imaging of Carbon Fibers

Scanning Electron Microscopy (SEM) images were used to characterize SCFs. Images were collected in either a Nova Nanolab 200 DualBeam SEM (FEI, Hillsboro, OR, USA) or a MIRA3 SEM (Tescan Orsay Holding, Brno-Kohoutovice, Czech Republic). An accelerating voltage of 2 kV or 3 kV and a current of 0.21 nA or 24 pA was used on the Nova or MIRA3, respectively. Both SEMs used an Everhart-Thornley detector for high-vacuum secondary electron imaging. Arrays were mounted on standard SEM pin stub mounts (16111, Ted Pella, Redding, CA, USA) using carbon tape (16073, Ted Pella, Redding, CA, USA) and gold sputtered for 60–120 seconds (11429, Structure Probe, Inc., West Chester, PA, USA).

1.5 Electrochemical Deposition of Polymer Coating

To lower impedance, a solution of 0.01 M 3,4-ethylenedioxythiophene (483028, Sigma-Aldrich, St. Louis, MO, USA) and 0.1 M sodium p-toluenesulfonate (152536, Sigma-Aldrich, St. Louis, MO, USA) was electrodeposited onto the exposed carbon of the SCFs by applying 600 pA/channel for 600 seconds to form a layer of poly(3,4-ethylene-dioxythiophene):sodium p-toluenesulfonate (PEDOT:pTS) (Green et al., 2012; Kozai et al., 2012; Patel et al., 2015, 2016).

1.6 Electrochemical Impedance Spectroscopy (EIS) and Cyclic Voltammetry (CV) Analysis

Electrochemical Impedance Spectroscopy (EIS) and Cyclic Voltammetry (CV) measurements were collected to characterize electrode fabrication steps and post-surgery viability. Three-electrode measurements were performed with a PGSTAT12 Autolab potentiostat (Metrohm / Eco Chemie, Utrecht, Netherlands) and vendor-supplied Nova software. SCFs were submerged in 1x phosphate buffered saline (PBS) (BP3994, Fisher, Waltham, MA, USA) in a small petri dish with an Ag|AgCl reference electrode (RE-5B, BASi, West Lafayette, IN, USA) and a stainless steel rod counter electrode, similar to the bone screw counter electrode used in brain electrophysiology experiments (Patel et al., 2015, 2016). To obtain EIS measurements, a 10 μV_{RMS} signal was applied from 10 Hz to 31 kHz. CV measurements were obtained by sweeping from 0.8 V to -0.6 V three times at a scan rate of 1 V/s. EIS and CV measurements were analyzed with custom MATLAB scripts (Mathworks, Natick, MA, USA). Fibers were rinsed in deionized water after measurement.

1.7 Bend Testing of Silicone-Embedded Carbon Fibers

Carbon fibers were embedded in medical grade silicone to test their bending characteristics. Custom alignment PCBs were used to align 8 bare carbon fibers at a 152.4 µm pitch. A CNC milled aluminum baseplate (Protolabs, Maple Plain, MN, USA) was designed with 6 oval depressions (1.8 mm x 1 mm, 0.6 mm depth) to serve as silicone molds. A holder for 6 alignment PCBs was printed with a Form 2 SLA 3D printer to center the fibers on each alignment PCB with corresponding silicone molds and submerge the fibers by 300–400 µm into the silicone. To build the testing devices, the molds on the baseplate were filled with silicone (A-103, Factor II, Lakeside, AZ, USA) and then degassed in a vacuum chamber for 20 minutes at -0.09 MPa. Six alignment PCBs with 8 carbon fibers each were attached to the 3D-printed holder and this device was then attached to the baseplate. The setup was then placed on a hotplate for 20 minutes at 110° C to cure the silicone. Once the silicone cured, fibers were cut at the edge of the alignment PCB with microsurgical scissors and the silicone-CF testing devices were gently removed from the baseplate with forceps. While the silicone-CF testing devices were primarily used in the bending experiments, in a small number of experiments CFSAs were tested to verify that the amount of silicone above the edge of the polyimide PCB exhibited the same properties as CFs embedded purely in silicone.

Carbon fiber bending experiments used a 0.75 mm diameter glass capillary (625000, A-M Systems, Sequim, WA, USA) to repeatedly bend the carbon fibers. Testing devices were placed on a level surface and secured with carbon tape. The glass capillary was secured to the end of a linear actuator (M-235.5DD, PI, Auburn, MA, USA) with a custom 3D-printed part. The actuator was aligned such that the movement of the capillary was perpendicular to the fibers and parallel to the surface of the silicone. The height of the glass capillary above the silicone was set to 40–60 µm with the help of a digital microscope placed perpendicularly to the fibers. The actuator was programmed so that the capillary swept back and forth over the fibers the desired number of times at a velocity of 17.09 mm/s and acceleration of 4.88 mm/s^2. One pass was considered the complete movement of the glass capillary from one end of the line of carbon fibers to another in a single direction. The percent of broken fibers on each device was collected at some combination of the experimental increments of 200, 1000, 2000, 6000, 8000, 10000, 20000, 30000, 40000, and 50000 passes.

1.8 Animal Surgery

All animal procedures were approved by the Institutional Animal Care and Use Committee. Electrophysiological recordings were collected from three locations in non-survival surgical procedures: rat CVN, feline DRG, and rat brain motor cortex. Prior to all surgeries, ground and reference wires (AGT05100, World Precision Instruments, Sarasota, FL, USA) were soldered to the interface PCB. Approximately 1 cm of wire length was exposed from insulation at each free end of the ground and reference wires. In preparation for surgical handling, the free end of the polyimide PCB in CFSAs was clamped by a set of nerve forceps such that the fibers pointed away from the forceps. Wire lengths of CFSAs were secured to the forceps with carbon tape.

1.8.1 Acute Rat Cervical Vagus Nerve (CVN) Surgery

The non-survival CVN procedures were performed on male Sprague-Dawley rats (0.36–0.62 kg, Charles River Laboratories, Wilmington, MA, USA), as detailed in Jiman et al., 2020 (N=22 for companion study, +1 additional animal in current study), using Flex Arrays (150–250 µm length SCFs). Isoflurane (Fluriso, VetOne, Boise, ID, USA) was used for initial anesthetic induction (5%) and maintenance (2–3%). Rats were placed on a heating pad (ReptiTherm, Zoo Med Laboratories, Inc., San Luis Obispo, CA, USA) and vitals were monitored (SurgiVet, Smiths Medical, Norwell, MA,

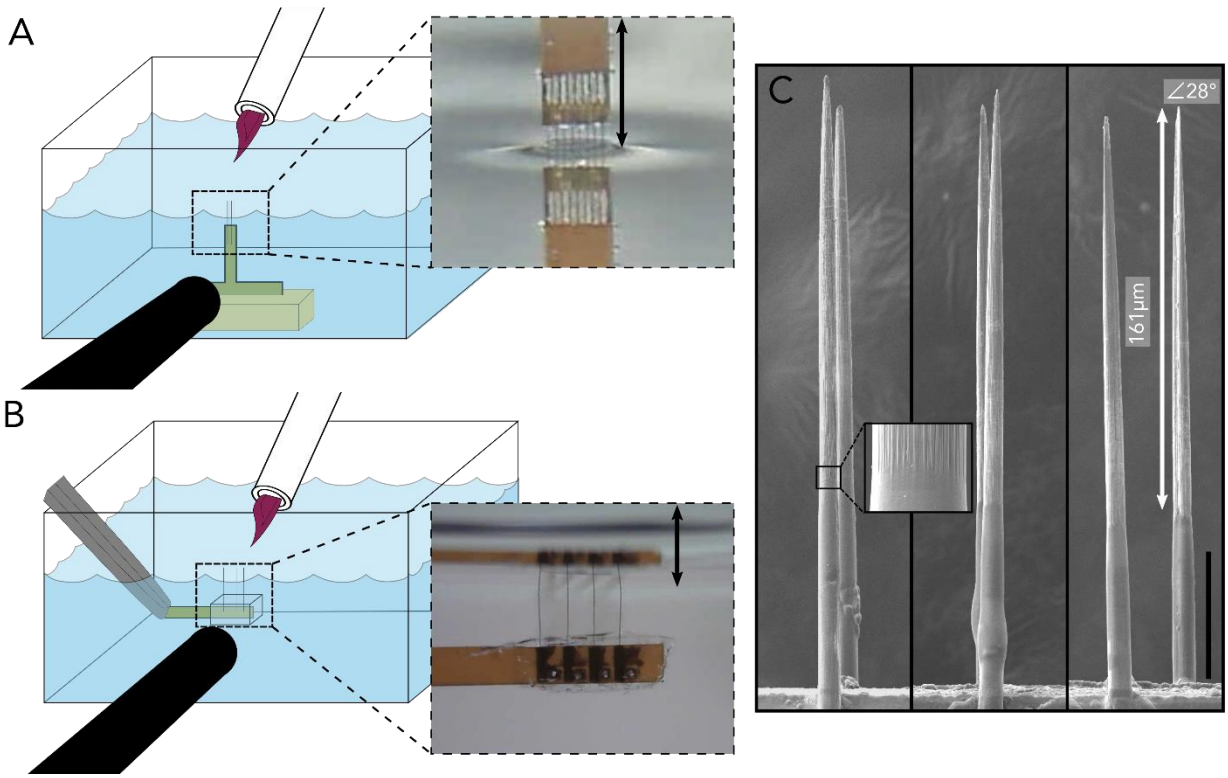

Figure 2. Blowtorch schematic for Flex Array (A) and CFSA (B). A) Flex Arrays are secured to the base of the water dish with putty and the water level is adjusted until the carbon fiber tips touch their reflection on the underside of the water surface (inset, black arrow denotes reflection). B) CFSAs are held with nerve forceps and lowered into the water dish until the carbon fiber tips touch their reflection on the underside of the water surface (inset, black arrow denotes reflection). With both arrays, a pen camera located outside the water dish views the carbon fiber reflection under the water surface to confirm that the carbon fibers are aligned to the water surface. A butane flame is passed over the water surface to sharpen the carbon fibers. C) Sharpened fibers have a smooth transition from parylene-c to bare carbon (inset). The representative sharpened carbon fiber on the right has 161 µm of carbon exposed from parylene-c (white arrow) and a tip angle of 28 degrees. Scale bar is 50 µm.

USA). The CVN was accessed through a midline ventral cervical incision. The cervical opening was maintained with retractors (17009-07, Fine Science Tools, Inc., Foster City, CA, USA). A dissection microscope and fine forceps (00632-11, Fine Science Tools, Inc., Foster City, CA, USA) were used for the isolation of approximately 10 mm of CVN from the carotid artery and surrounding tissue. The CVN was lifted (~2 mm) on to a custom 3D-printed nerve-holder to facilitate carbon fiber insertion.

The Flex Array was positioned over the elevated CVN using a 3-axis micromanipulator (KITE-R, World Precision Instruments, Sarasota, FL, USA) secured to an optical breadboard (MB1218, Thorlabs, Inc., Newton, NJ, USA). The ground wire for the Flex Array was inserted subcutaneously in the cervical area and the reference wire was placed in the tissue of the cervical cavity. A small pen-shaped camera (MS100, Teslong, Shenzhen, China) was aligned at the edge of the nerve-holder to visualize the carbon fibers during insertion. Prior to recording, the heating pad and dissection microscopy were disconnected to reduce electrical noise. The nerve was rinsed with saline (0.9% NaCl, Baxter International, Inc., Deerfield, IL, USA) and the Flex Array carbon fibers were lowered and inserted into the CVN.

1.8.2 Acute Feline Dorsal Root Ganglion Surgery

Three adult, domestic, short-hair male felines (4.0–5.6 kg, 1.3–1.4 years, Marshall BioResources, North Rose, NY, USA) were used for the DRG experiments with Flex Arrays (150–250 µm length SCFs). One feline (5.2 kg, 1.2 years) was used for the DRG experiment with a CFSA (375–475 µm length SCFs). Flex Arrays were previously used in CVN experiments. The animals were anesthetized with an intramuscular injection of ketamine (6.6 mg/kg), butorphanol (0.66 mg/kg), and dexmedetomidine (0.011 mg/kg). Animals were intubated and maintained on isoflurane (0.5–4%) and vitals were monitored (respiratory rate, heart rate, end-tidal CO_2, O_2, perfusion, temperature, and intra-arterial blood pressure). For fluid infusion and pressure monitoring, a 3.5 Fr dual-lumen catheter was inserted to the bladder through the urethra. A midline dorsal incision was made to expose the L7 to S3 vertebrae. A laminectomy was performed to access the S1–S2 DRG. After experimentation, animals were transitioned from isoflurane to intravenous alpha-chloralose (70 mg/kg induction and 20 mg/kg maintenance) for the

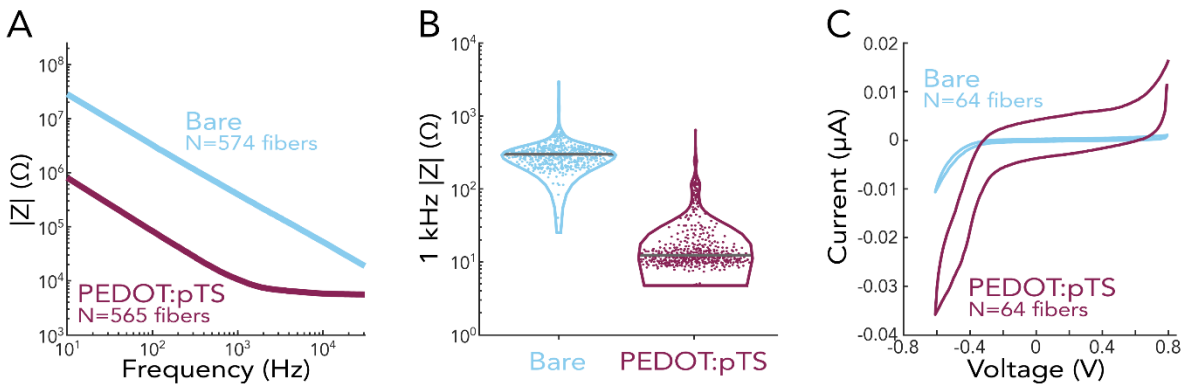

Figure 3. Electrochemical impedance spectroscopy and cyclic voltammetry analysis of bare sharpened carbon fibers (SCFs), shown in blue, and PEDOT:pTS coated SCFs, shown in purple. A) Impedance magnitude frequency spectrogram of bare SCFs (N=574) and PEDOT:pTS coated SCFs (N=565). B) Violin plot of 1 kHz impedance magnitudes of bare SCFs (N=574) and PEDOT:pTS coated SCFs (N=565). Mean 1 kHz impedance magnitude of bare and PEDOT:pTS coated SCFs was 334.8 ± 243.2 kΩ and 32.3 ± 55.7 kΩ, respectively. C) CV curves of bare SCFs (N=64) and PEDOT:pTS coated SCFs (N=64). The cathodal charge storage capacity increased from 15.2 ± 5.4 μC/cm2 to 255.0 ± 148.6 μC/cm2 once bare SCFs were coated with PEDOT:pTS.

remainder of the experiment. Buprenorphine was provided subcutaneously every 8 to 12 hours as analgesia.

The Flex Array or CFSA was held in place with a clamp or nerve forceps and lowered into the surgical site using a linear actuator or micromanipulator, respectively. The ground wire was placed subcutaneously at a distant location and the reference wire was placed near the spinal nerve. Insertion into the S1 or S2 DRG was visualized with a small pen-shaped camera (MS100, Teslong, Shenzhen, China). After insertion, impedances were recorded at 1 kHz. For brushing trials with the Flex Arrays, the scrotum was brushed with a cotton-tip applicator for 10 seconds following a period of no brushing for 10 seconds, repeated for 60 seconds total. For bladder trials with the Flex Array, saline was infused into an empty bladder at 2 mL/min until either an elevated bladder pressure occurred or urine leaking was observed. CFSA trials consisted of exploratory perineal brushing and baseline recordings.

1.8.3 Acute Rat Cortical Surgery

Four adult male Sprague Dawley rats (0.3–0.4 kg, Charles Rivers Laboratories, Wilmington, MA, USA) were used for the acute cortical experiments with CFSAs (75–1075 μm length SCFs). Two animals were excluded due to surgical complications unrelated to device features. Animals received carprofen (5 mg/kg) and were anesthetized with ketamine/xylazine (90/10 mg/kg) for induction and ketamine (30 mg/kg) for maintenance. Rat vitals were monitored during surgery using a pulse-oximeter and rectal temperature probe. Surgical preparation for carbon fiber insertion is detailed in Welle et al., 2020. In summary, the skull surface was cleaned and a hole drilled (19008-07, Fine Science Tools, Foster City, CA, USA) in the posterior edge of the skull for the placement of a bone screw (19010-00, Fine Science Tools, Foster City, CA, USA). A 2.5 mm by 2.5 mm craniotomy was drilled over the right hemisphere motor cortex (Paxinos & Watson, 2007). The CFSA was attached to a stereotactic manipulator and aligned over the craniotomy along the anterior-posterior axis. The exposed section of the ground and reference wires were wound around the grounding bone screw. A dural slit was made in the center of the craniotomy. The CFSA was manually lowered and the fibers were driven into the brain until the final target depth (0.775–1.180 mm) in layer V (Skoglund, Pascher, & Berthold, 1997) was reached.

1.9 Electrophysiology Recording

Neural recordings from the rat CVN and feline DRG were collected using a Grapevine Neural Interface Processor (Ripple LLC, Salt Lake City, UT, USA). Electrophysiological signals were recorded at a sampling rate of 30 kHz. Impedances were measured during rat CVN experiments at 1 kHz in saline before the procedure and in the nerve immediately after insertion. Impedances were measured during the majority of feline DRG experiments at 1 kHz immediately after insertion. At least 5 minutes, 10 minutes, or 1 minute of recordings were obtained for the rat CVN, feline DRG bladder experiments, and feline DRG brushing experiments, respectively.

Brain electrophysiology recordings were collected using a ZC16 headstage, RA16PA pre-amplifier, and RX5 Pentusa base station (Tucker-Davis Technologies, Alachua, FL, USA). Data was sampled at a rate of 25 kHz, high-pass filtered at 2.2 Hz, and anti-alias filtered at 7.5 kHz. Each recording session lasted at least 3 minutes.

1.10 Analysis of Neural Recordings

Principle component analysis of neural recordings was conducted in Offline Sorter (OFS, Plexon, Dallas, TX, USA) to isolate neural clusters. The electrophysiology signals were filtered with a band-pass filter at 300–10,000 Hz and a threshold was manually set just below the noise floor. A trained operator manually identified neural clusters from the

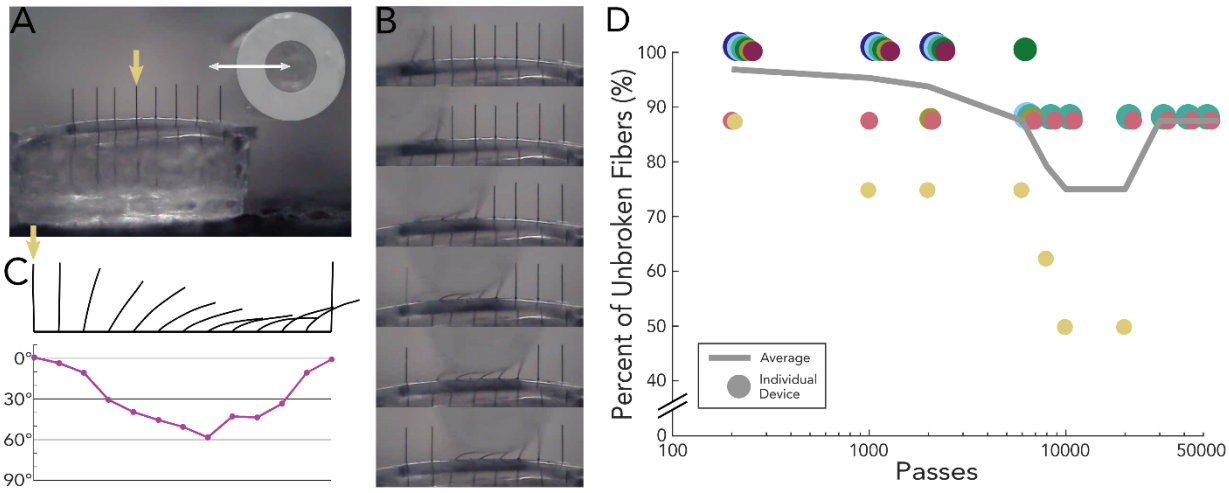

Figure 4. Bend test of silicone-embedded carbon fibers. A) Bend test setup with a silicone-embedded carbon fiber testing device and a 0.75 mm diameter glass capillary. The glass capillary, outlined in light grey, passes over the carbon fibers to bend them, with a complete run from end to end counting as one pass. B) Still images from a video shown in (A) and in Supplemental Video 1 of the glass capillary part way through one pass over the carbon fibers. The carbon fibers are shown bending as the capillary passes over them. C) Top: Outlines of a single fiber, indicated in (A) by the yellow arrow, bending as the glass capillary passes over. Bottom: Corresponding angle measurements from each still image outline of the fiber. On average, carbon fibers deflected 50.9 ± 6.2 degrees from the vertical position (N=23 fibers, 3 devices). D) Bend test data showing the percent of unbroken fibers plotted against the number of glass capillary passes. Each device is shown as an individually colored circle and the average across all devices is shown as the solid line. After 50,000 passes, 87.5% of fibers remained unbroken.

vagus nerve and DRG recordings. Clusters from the brain were identified in OFS using the semi-automated method described in Welle et al., 2020. Sorted clusters were identified by unique amplitude, waveform shape, inter-spike interval, and response to physiological signals, such as breathing rate. MATLAB (MathWorks, Natick, MA, USA) was used to analyze the sorted clusters. Firing rates of bladder clusters were calculated with a bin duration of 1 second and correlated to bladder pressure until the maximum bladder pressure (Ouyang, Sperry, Barrera, & Bruns, 2019). The signal-to-noise ratio (SNR) was calculated using the mean peak-to-peak amplitude (V_{pp}) of a sorted cluster and the standard deviation of at least 500 ms of noise from the respective recording [SNR = V_{pp} / (2 * standard deviation of noise)]. When appropriate, values are presented as mean ± standard deviation (SD).

Results

2.1 Analysis of Sharpened Carbon Fibers

A blowtorch method for sharpening <500 µm linear carbon fiber arrays was developed to facilitate consistent insertion success in peripheral targets (Figure 2A, B). Example SCFs attached to Flex Arrays are shown in Figure 2C. Prior to blowtorching, carbon fibers were manually cut using microsurgical scissors to roughly 200 µm in length. After blowtorching, SEM analysis confirmed the average length of SCFs as 223.7 ± 18.9 µm (N=32 fibers). SCFs exhibited an average tip angle of 72.3 ± 33.5 degrees with a 146.8 ± 17.7 µm length of carbon exposed from parylene-c insulation, constituting an active recording site of 2734.5 ± 402.5 μm^2 surface area (Figure 2C). The parylene-c transition between the exposed and insulated carbon appeared smooth on all imaged fibers (Figure 2C inset).

After sharpening, the electrodes were coated with poly(3,4-ethylene-dioxythiophene):sodium p-toluenesulfonate (PEDOT:pTS). The impedance magnitude frequency spectrum of PEDOT:pTS coated SCFs showed the largest shift in impedance magnitude at lower frequencies as compared to bare SCFs (Figure 3A). SCFs of 200 µm length without PEDOT:pTS coating exhibited an average 1 kHz impedance ($|Z|_{1kHz}$) of 334.8 ± 243.2 kΩ and a median $|Z|_{1kHz}$ of 298.6 kΩ (N=574 fibers). Once coated with PEDOT:pTS, SCFs exhibited an average $|Z|_{1kHz}$ of 32.3 ± 55.7 kΩ and a median $|Z|_{1kHz}$ of 12.4 kΩ (N=565 fibers) (Figure 3B). Therefore, coating the active SCF recording site with PEDOT:pTS contributed to a 90% decrease in average $|Z|_{1kHz}$ (Figure 3B). Correspondingly, the cathodal charge storage capacity of SCFs increased from 15.2 ± 5.4 $\mu C/cm^2$ to 255.0 ± 148.6 $\mu C/cm^2$ (N=64 fibers), calculated at a sweep rate of 1 V/s, after PEDOT:pTS deposition (Figure 3C).

2.2 Robustness Testing of Silicone-Embedded Carbon Fibers

We embedded carbon fibers in medical grade silicone to harness the intrinsic compliance of carbon fibers (Kozai et al., 2012; Woods et al., 2020) and provide strain relief at the junction of SCFs and the polyimide PCB, therefore minimizing the eventual breakage seen on Flex Arrays after

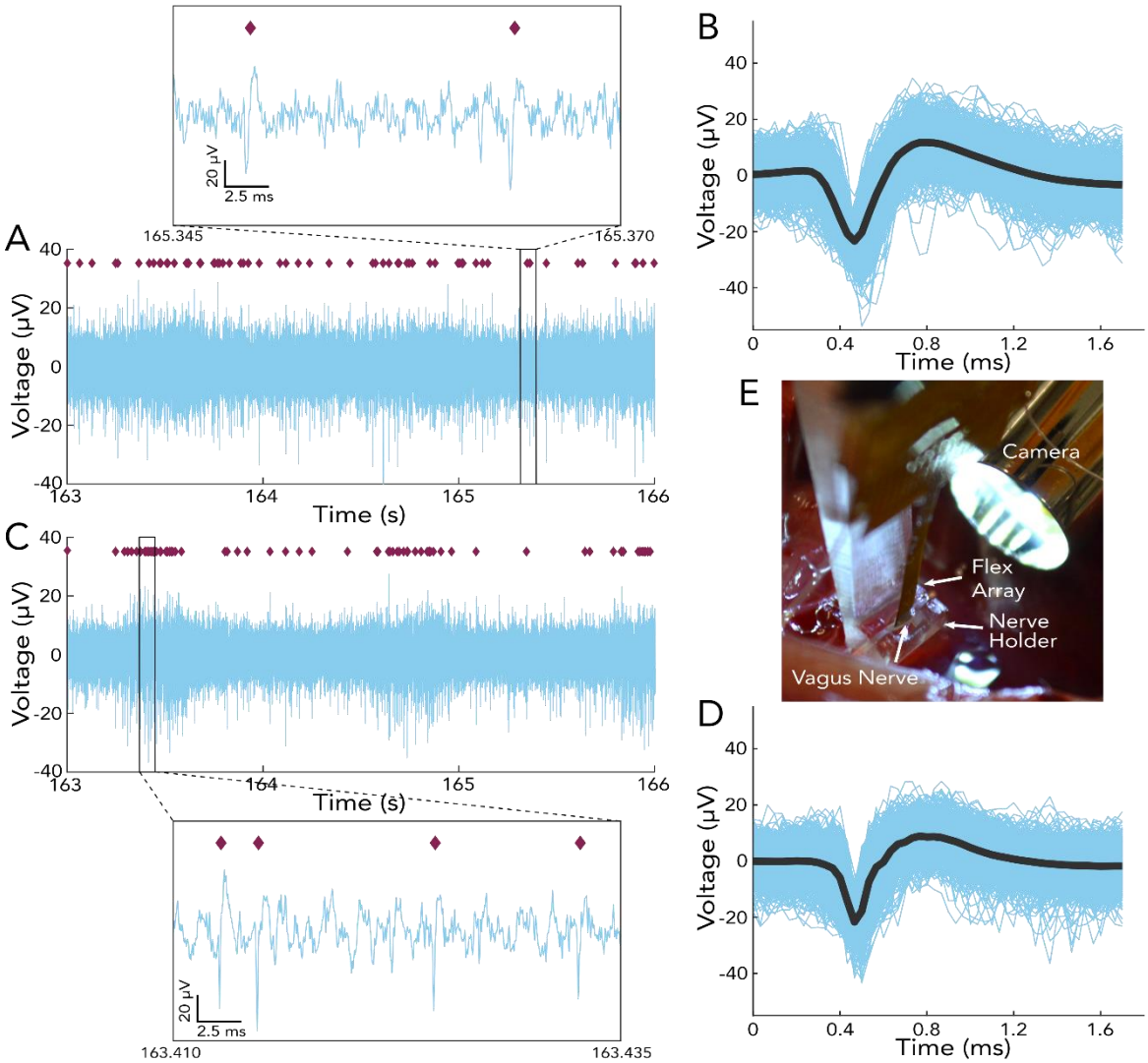

Figure 5. Neural activity recorded from a rat cervical vagus nerve (CVN) with sharpened carbon fibers (SCFs) on a Flex Array, representative of the larger data set shown in Jiman et al., 2020. A and C) Three seconds of filtered data recorded on two SCFs. 25 µs of data is shown in the insets of each raw trace. B and D) Corresponding neural cluster indicated in (A) and (C) by purple diamond with the mean cluster waveform shown by gray solid line. B) The mean V_{pp} of the neural cluster was 139.9 ± 26.4 µV. D) The mean V_{pp} of the neural cluster was 122.8 ± 24.3 µV. E) Surgical setup showing the CVN lifted by the nerve holder while the camera is used to visually align the Flex Array.

repeated insertions. Bend tests were conducted on silicone-embedded carbon fibers, with and without attachment to an embedded polyimide PCB, using a 0.75 mm diameter glass capillary (Figures 4A, C, Supplemental Video 1, Supplemental Video 2). On average, carbon fibers deflected 50.9 ± 6.2 degrees from the vertical position (N=23 fibers, 3 devices), representatively shown in Figure 4B. The maximum measured fiber deflection from vertical without fracture was 71.6 degrees. We observed that an average of 93.8% fibers (N=58/62) did not break after 2,000 bends (passes of the capillary) during continuous fatigue testing (Figure 4D). After 50,000 passes, 87.5% of fibers remained unbroken (N=14/16). This robustness was similarly observed on carbon fibers embedded in at least 150 µm of silicone when attached to an embedded polyimide PCB (Woods et al., 2020, Supplemental Video 2).

2.3 Acute Electrophysiology Recordings from Rat Cervical Vagus Nerve (CVN)

We tested the ability of SCFs to insert into the small diameter (300–500 µm) rat CVN and record. Six Flex Arrays with SCFs of 200–250 µm length, as represented in Figure 1C, were inserted into the left CVN of 22 Sprague-Dawley rats (Figure 5E, Supplemental Video 3). Detailed characterization of the population recordings is presented in a companion study by Jiman *et al.* 2020. In all experiments, we visually observed successful insertion of all SCFs into the vagus nerve after an average of 2.3 insertion attempts. The functional SCFs

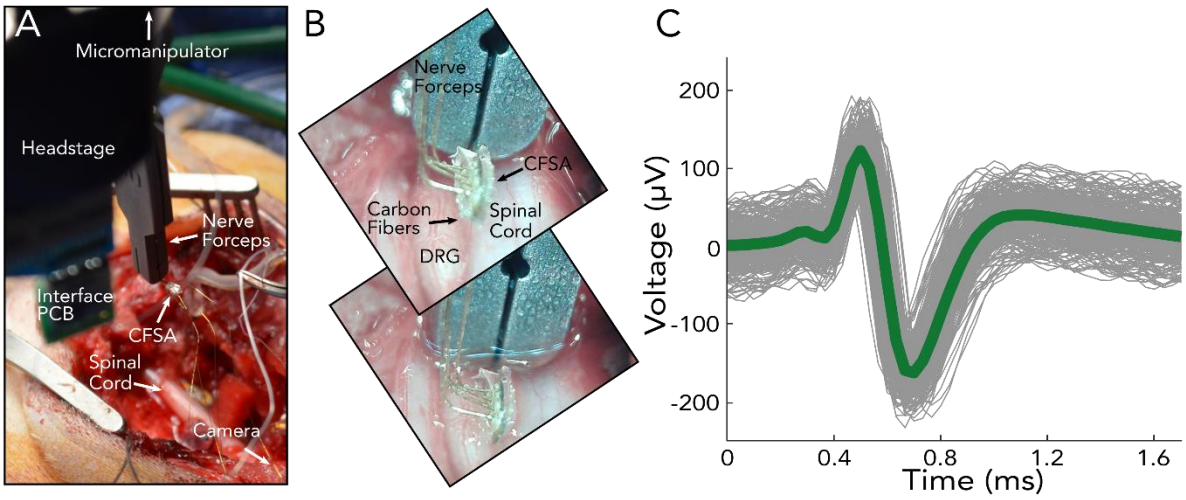

Figure 6. CFSA experiment in feline dorsal root ganglia (DRG). A) Surgical setup showing the CFSA, held by nerve forceps, and interface PCB connected to a headstage lowered into the surgical cavity with a micromanipulator. The CFSA is inserted into the DRG located below the visible spinal cord. The camera is positioned parallel to the spinal cord to the right of the surgical cavity. B) CFSA, held by nerve forceps, as seen by the surgical camera before (top) and after (bottom) insertion into the DRG. C) Neural cluster associated with spontaneous activity recorded in the DRG with the CFSA. The cluster has a mean V_{pp} of 298.8 ± 15.5 µV and SNR of 6.5. The mean waveform shape is shown in thick green line.

(defined as $|Z|_{1kHz}$ < 1 MΩ) had an average $|Z|_{1kHz}$ of 70.8 ± 81.9 kΩ after insertion (N=326 fibers). Neural activity was recorded on 51.2% of the functional SCFs. Manual sorting and a mixture of Gaussians sorting methods were applied in principal component space to classify neural activity into clusters of distinct bipolar waveform shape. Across the 326 functional SCFs, 174 sorted neural clusters were detected. The neural clusters had a mean V_{pp} of 30.7 ± 11.43 µV and a mean SNR of 3.52 ± 1.0. We observed that 19.8% of functional SCFs recorded neural clusters with SNRs > 4. The maximum mean V_{pp} was found to be 91.72 µV (Jiman et al., 2020).

Representative electrophysiological recordings of spontaneous vagus nerve activity is shown in Figure 5. Sixteen SCFs were determined functional and had an average $|Z|_{1kHz}$ of 25.3 ± 10.9 kΩ after insertion into the vagus nerve. Sorting analysis identified neural clusters on 3 of 16 functional SCFs in this example experiment. Neural data from 2 functional SCFs are shown in Figure 5A and C. The corresponding neural cluster from each functional SCF had a mean V_{pp} of 139.9 ± 26.4 µV and 122.8 ± 24.3 µV (Figure 5B, D). Across all 3 SCFs, we found that the waveform V_{pp} of clusters ranged from 18.5 µV to 108.5 µV. The sorted neural clusters had a mean V_{pp} of 41.8 ± 6.8 µV and an average median V_{pp} of 41.0 µV. Clusters from this representative experiment had a mean SNR of 4.1 ± 0.08.

2.4 Acute Electrophysiology Recordings from Feline Dorsal Root Ganglion

We sought to discover whether it is possible to insert SCFs of short length (150–250 µm) into feline DRG with minimal external force during insertion. We inserted 16-channel Flex Arrays with 150–250 µm length SCFs into the S1 DRG of 3 felines (Figure 7A, B) and a 4-channel CFSA with 375–475 µm length SCFs into the S2 DRG of 1 feline (Figure 6A, B). In each experiment, the array was manually lowered with a micromanipulator until SCFs were visually inserted in tissue. Functional SCFs ($|Z|_{1kHz}$ < 1 MΩ) had an average $|Z|_{1kHz}$ of 26.9 ± 7.4 kΩ in the DRG immediately after insertion (N=30 fibers).

Despite the large recording surface area, neural clusters were observed on 32 of 52 total inserted SCFs (N=4 felines; 3 Flex Arrays; 1 CFSA), and 27 of 30 functional ($|Z|_{1kHz}$ < 100 kΩ) SCFs (N=3 felines; 2 Flex Arrays; 1 CFSA). Impedance data was not recorded on one feline and excluded from the functional SCF count.

Our offline sorting analysis of recorded neural activity identified 73 neural clusters across all feline experiments with an average of 1.8 ± 0.9 clusters per SCF. Clusters were classified as either spontaneous or driven. Spontaneous neural activity was sorted into clusters associated with breathing (breathing clusters), clusters unlinked to obvious physiological signal (spontaneous clusters, Figure 6C), and clusters containing multiple units (multi-unit clusters). Driven clusters responded to the experimental variables of perineal or scrotal brushing (brushing clusters, Figure 7C, D) or saline-infusion of the bladder (bladder clusters, Figure 7E, F). Across all experiments, we classified 16.2% of clusters as breathing, 43.2% as spontaneous, and 16.2% as multi-unit, 14.9% as brushing, and 9.5% as bladder clusters.

Breathing clusters depicted rising and falling amplitudes, in addition to bursting patterns. We believe the observed changes in amplitude were likely due to micromotion shifts in SCF

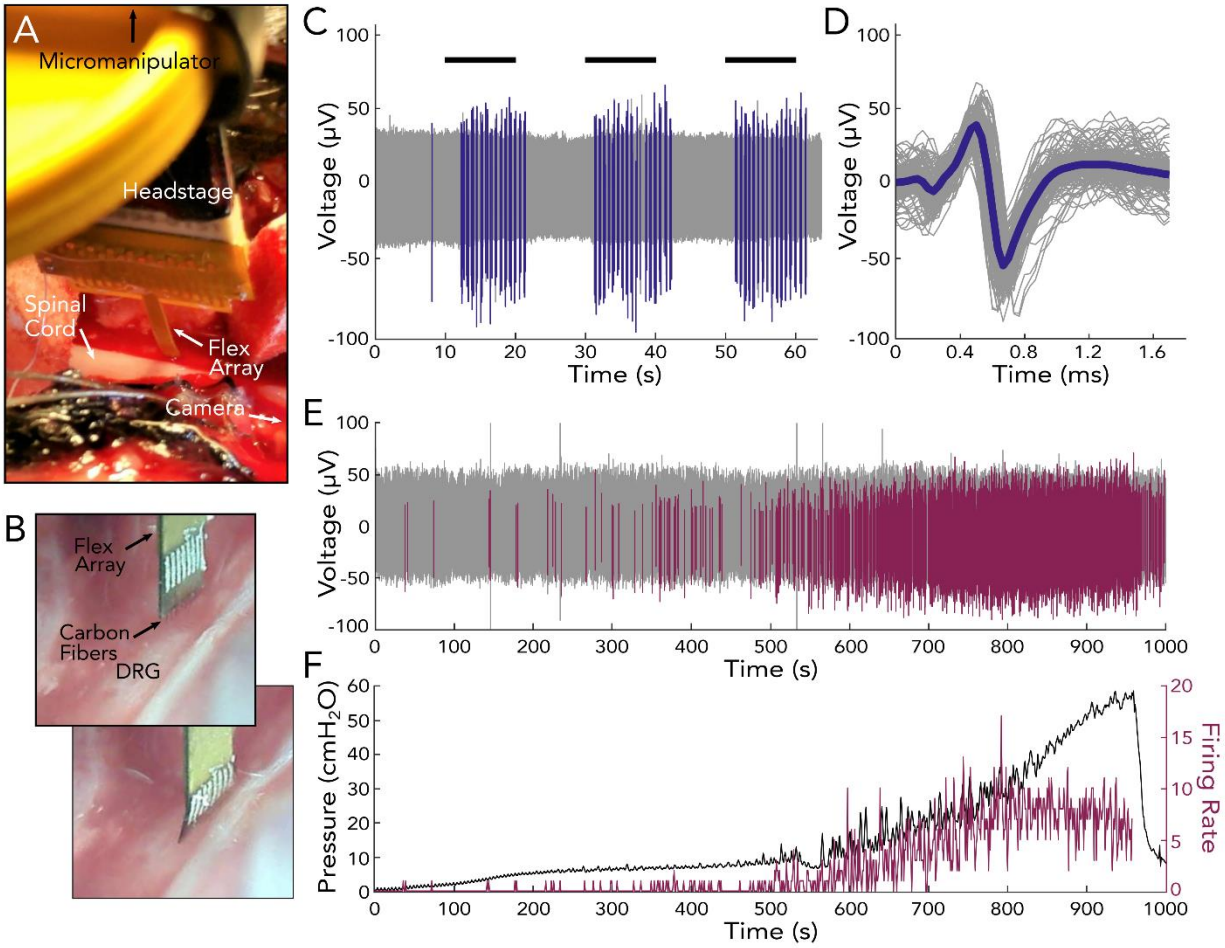

Figure 7. Flex Array experiments in feline dorsal root ganglia (DRG). A) Surgical setup showing the Flex Array connected to a headstage lowered into the surgical cavity with a micromanipulator. The Flex Array is inserted into the DRG located above the visible spinal cord. The camera is positioned parallel to the spinal cord to the right of the Flex Array. B) Flex Array as seen by the surgical camera before (top) and after (bottom) insertion into the DRG. C) Neural activity in response to scrotal brushing. Brushing time denoted by horizontal black lines. Waveforms in the neural cluster associated with brushing are colored blue. D) Brushing cluster from (C) with mean V_{pp} of 108.7 ± 11.0 µV and SNR of 6.0. Mean waveform shape is shown in thick blue line. E) Neural activity associated with bladder filling. Waveforms in the neural cluster associated with brushing are colored purple. F) Bladder pressure (left axis) and firing rate (right axis) of bladder cluster in (E).

position with respect to the neuron as the animal's body shifted slightly with each breath. The V_{pp} of breathing clusters ranged from 41.4 µV to 186.7 µV, with a mean V_{pp} of 84.4 ± 16.8 µV and a mean SNR of 7.0 ± 3.7 (N=12 clusters; 3 Flex Arrays). Spontaneous clusters did not obviously track with breathing or other physiological signals. The mean V_{pp} of spontaneous clusters was 115.9 ± 16.6 µV and a mean SNR of 7.9 ± 6.0 (N=32 clusters; 3 Flex Arrays; 1 CFSA). Figure 6C shows an example spontaneous cluster recorded from the CFSA with a mean V_{pp} of 298.8 ± 15.5 µV and SNR of 6.5. Multi-unit clusters contained clear neural activity, but we were unable to differentiate spontaneous clusters. Multi-unit clusters had a mean V_{pp} of 34.2 ± 6.3 µV and a mean SNR of 4.7 ± 1.2 (N=12 clusters; 1 Flex Array).

To further verify that spikes were neural in origin, we recorded neural activity in response to cutaneous brushing and bladder filling. In 2 of 3 experiments with Flex Arrays recording from the S1 DRG, we recorded neural activity corresponding to the cutaneous response to scrotal brushing. We observed 10 clusters on 8 SCFs with bursting activity during the 10 second brushing intervals. Example neural activity from a brushing experiment is shown in Figure 7C. The corresponding brushing cluster, shown in Figure 7D, has a mean V_{pp} of 108.7 ± 11.0 µV and SNR of 6.0. The mean V_{pp} of all brushing clusters was 152.4 ± 13.5 µV and the mean SNR was 7.1 ± 4.5 (N=10 clusters; 2 Flex Arrays). We also recorded a single brushing cluster in response to perineal brushing on a CFSA SCF in one experiment. The mean V_{pp} of the cluster was 219.5 ± 54.1 µV and the mean SNR was 18.9 (N=1 cluster; 1 CFSA)

We also observed neural activity that contained physiologically-relevant signals of bladder pressure in

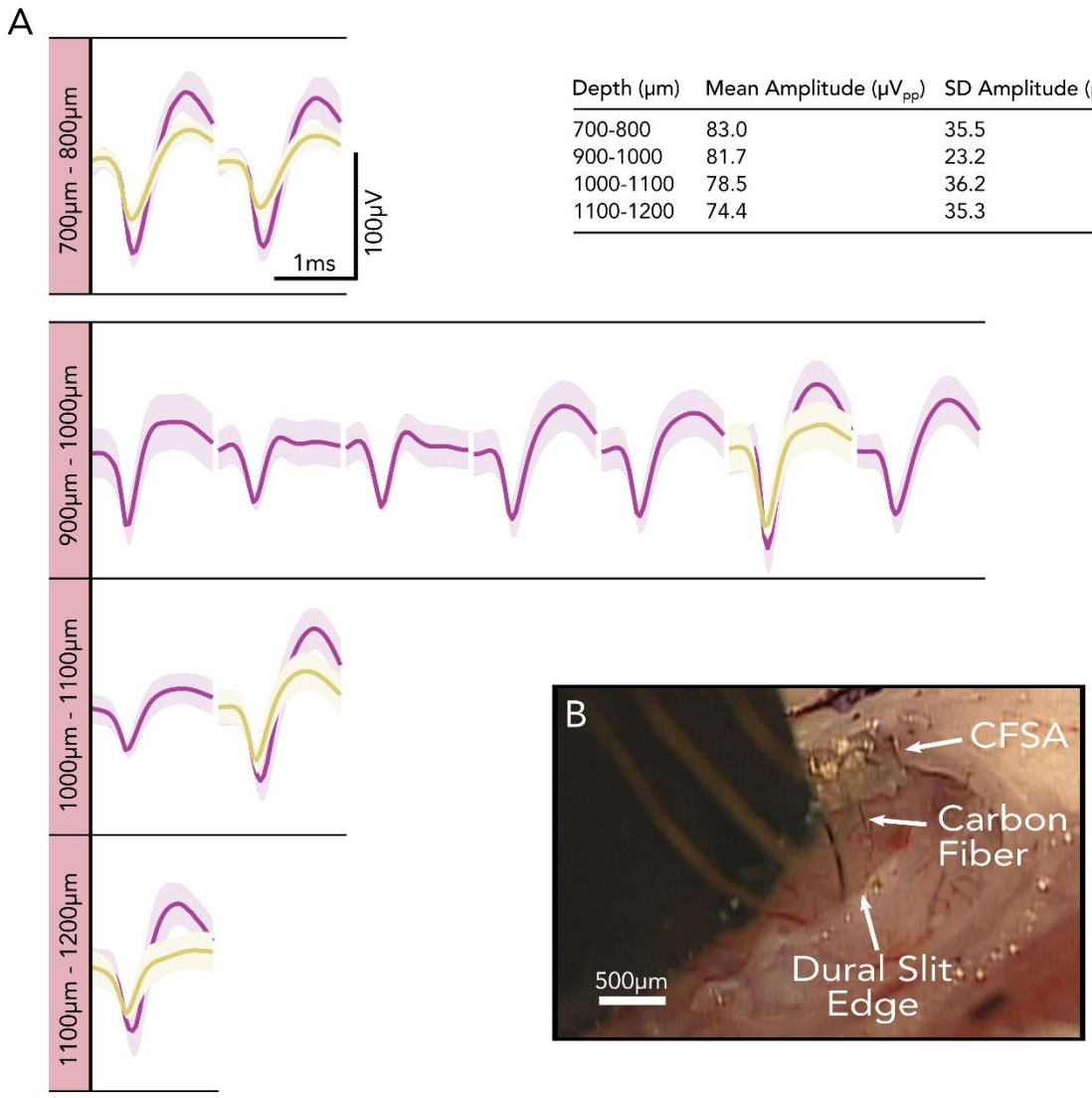

Depth (µm)	Mean Amplitude (μV_{pp})	SD Amplitude (μV_{pp})
700-800	83.0	35.5
900-1000	81.7	23.2
1000-1100	78.5	36.2
1100-1200	74.4	35.3

Figure 8. Electrophysiology recorded from sharpened carbon fibers (SCFs) on CFSAs in the rat motor cortex. A) Neural units recorded at varying depth increments. The units were recorded on 6 SCFs across 3 devices during 7 independent insertions into the brain. Each unit, or overlapping units, was recorded from a single SCF during one insertion. A summary of the mean amplitude and standard deviation of neural units at each depth is shown in the inset table. B) Surgical setup of CFSA insertion into the brain within the opening of a dural slit.

response to bladder filling. Across all experiments, the firing rates of 7 neural clusters were found to correlate with bladder pressure during the bladder filling procedure. A representative bladder cluster is shown in Figure 7E and 7F. Correlation coefficients between bladder pressure and firing rate were calculated for each bladder cluster. The correlation coefficients were between 0.23 and 0.82, with a median of 0.70. The mean correlation coefficient of the 7 clusters with their respective bladder pressure was 0.61 ± 0.21. The V_{pp} of the bladder clusters were between 32.1 µV and 190.4 µV, with a mean V_{pp} of 86.8 ± 14.1 µV and a mean SNR of 10.3 ± 6.3 (N=7 clusters, 3 Flex Arrays).

We observed that several clusters recorded on the Flex Array appeared on multiple adjacent SCFs. These units fulfilled our metrics for being a sortable cluster in terms of amplitude, signal width, and inter-spike-interval, but appeared concurrently on multiple consecutive channels. In one instance, a breathing cluster was seen on four SCFs in a 2 x 2 geometry on a Flex Array, spanning a distance of 141 µm between diagonal SCFs.

2.5 Acute Electrophysiology Recordings from Rat Cortex

SCFs on CFSAs of length 750 µm to 1075 µm were found to self-insert into dura-free brain tissue from depths of 775 µm to 1180 µm (Figure 8B, Supplemental Video 4). In total, 17 sortable single units were recorded from 6 SCFs across 3 devices during 7 independent insertions into the brain (Figure

8A). The mean V_{pp} was found to decrease as cortical depth increased (Figure 8 table). The overall mean V_{pp} was 80.7 ± 27.5 µV and the largest recorded unit amplitude was 126 µV.

Discussion

Here, we demonstrate the capabilities of sharpened carbon fiber (SFC) arrays for neural interfacing with targets in the central and peripheral nervous systems. The array presented here represents, to our knowledge, the first stiff, penetrating, carbon fiber array made robust with silicone embedding.

SCFs allowed for easy penetration into multiple neural structures of varying stiffness and geometry. Initial insertion attempts in the small diameter (300–500 µm) rat cervical vagus nerve (CVN) with the previously reported conventional blunt-tipped carbon fiber electrodes (Welle et al., 2020) yielded inconsistent or unsuccessful insertion, and surgeons often resorted to slitting the epineurium to ensure penetration into the nerve. However, short (< 250 µm) SCFs consistently and successfully inserted into the CVN. Additionally, successful insertion was achieved in the feline dorsal root ganglia (DRG), which is known to have a thick epineurium layer of 50–100 µm (Ostrowski, Sperry, Kulik, & Bruns, 2017; Sperry et al., 2018), without the assistance of the pneumatic inserter used by the Utah Array (Blackrock Microsystems, Salt Lake, City, UT, USA). In the brain, blunt-tipped carbon fibers previously relied upon insertion assistors, such as temporary stiffening agents or a silicon backbone, to insert into dura-free brain at lengths greater than 500 µm (Patel et al., 2015; Welle et al., 2020). Despite a diameter of only 6.8 µm, SCFs inserted without assistance into dura-free rat brain at lengths up to 1075 µm. Longer SCFs were not tested here but may still self-insert.

Silicone-embedded carbon fibers survived repeated bending, indicating a potential for robust surgical handling unlike what is typically seen for silicon, glass-encapsulated, or other metal penetrating electrodes (Woods et al., 2020). Slight instrument adjustments in the surgical space often translated into movement at the Flex Array–nerve interface extreme enough for total carbon fiber breakage. Biological motion surrounding peripheral nerve interfaces is likely more significant to the breakage of intraneural electrodes than the motion in the brain is for penetrating brain electrodes. This array harnesses the intrinsic compliance of carbon fibers and demonstrates a capability to withstand the long-term fatigue that a peripheral nerve interface is likely to experience. The small geometry of the silicone-embedded array of sharpened carbon fibers uniquely combines a flat backing with penetrating electrodes, similar to the Utah Slanted Electrode Array (USEA, Branner & Normann, 2000), but at a sub-cellular size and with biocompatible materials.

The blowtorch sharpening of carbon fibers resulted in a low-impedance electrode well within the range relevant for electrophysiology recording (Moffitt & McIntyre, 2005). While SCFs had a 10.6 times larger surface area than laser cut carbon fibers (2735 μm^2, 257 μm^2, respectively) from Welle et al., 2020, blowtorching resulted in only a 1.7 times increase in 1 kHz impedance from laser cut carbon fibers (32 kΩ , 19 kΩ, respectively). Despite the low 1 kHz impedance, it was unclear if the larger surface area would affect recording ability. We experimented with SCFs in rat CVN, feline DRG, and rat cortex, and recoded clear neural clusters from all locations. The amplitudes of neural clusters recorded from small, myelinated A fibers and unmyelinated C fibers within the rat CVN were predictably often lower than those recorded from cell bodies and axons within the feline DRG or rat cortex. The mean amplitudes of spontaneous neural clusters from the rat CVN, feline DRG, and rat cortex were 41.8 µV, 115.9 µV, and 80.7 µV, respectively. The smaller amplitude of neural clusters from the rat cortex recorded here as compared to our previous studies may be due to the larger surface area of the sharpened arrays (Patel et al., 2016; Welle et al., 2020). In addition to spontaneous activity, we recorded neural activity from the feline DRG corresponding to bladder pressure (86.8 ± 14.1 µV) and cutaneous brushing (152.4 ± 13.5 µV). The bladder clusters correlated to bladder pressure with a mean correlation coefficient of 0.61. While encouraging preliminary work, we did not exhaust the procedures available to us in order to drive every possible unit in the proximity of the SCFs in the feline DRG. This does not represent a definitive list of capabilities of this device. To the best of our knowledge, this is the first example of carbon fiber electrode recordings in feline DRG.

The design presented here could be beneficial for broad medical applications of peripheral nerve interfaces, such as control of hypertension (Ntiloudi, Zanos, Gatzoulis, Karvounis, & Giannakoulas, 2019), or the digestive system (Panda et al., 2020). The ability to record high quality signal units would improve the precision of many of these efforts while also allowing for novel studies of *in vivo* neurophysiology. Carbon fiber arrays have previously demonstrated a minimal scarring response in brain (Kozai et al., 2012; Patel et al., 2020, 2016; Welle et al., 2020), and other carbon composite electrodes have previously shown minimal scarring in nerve (McCallum et al., 2017). Additionally, carbon fiber electrodes have been shown to record high SNR single units on single channels in the brain (K. Wang et al., 2019). Due to their small size, carbon electrodes are more likely to land closer to regions of high electric field (Furniturewalla, Rustogi, Patrick, & Judy, 2019). The penetration capabilities observed here for the vagus nerve is of interest for diverse clinical effects in a range of conditions (Settell et al., 2020) as well as emerging applications such as monitoring cytokines (Zanos et al., 2018). The ability to penetrate DRG suggests that these probes may be useful for other vertebrate ganglia such as the nodose ganglia (Bielefeldt, Zhong, Koerber, & Davis, 2006; Clerc & Mei,

1983), invertebrate ganglia such as Aplysia (Lyttle, Gill, Shaw, Thomas, & Chiel, 2017), or insect nervous systems (Nizampatnam, Saha, Chandak, & Raman, 2018). In addition, the mechanical robustness in a soft substrate makes these arrays ideal candidates for long-term studies in large animal models (Fisher et al., 2014; Khurram et al., 2017).

Carbon fibers have traditionally been used primarily in the brain, for both electrophysiology and chemical sensing (Schwerdt, Shimazu, et al., 2017). The ability to insert individuated, sharpened fibers as an array without assistance may enable larger channel count arrays of small stiff electrodes (Obaid et al., 2020; Saleh et al., 2019). Sharpened carbon fibers arrays may be useful for shuttling softer cellular scale electrodes deeper into brain tissue (Luan et al., 2017; X. Wang et al., 2020). The smooth parylene transition after blowtorching also creates a favorable surface for electroplating, for example with platinum iridium (Cassar et al., 2019). With this larger surface area, we were able to record neural units. However, the size of these units would likely increase with a smaller surface area electrode (Moffitt & McIntyre, 2005). This might be achieved, for example, by electrochemical etching (El-Giar & Wipf, 2006; Khani & Wipf, 2019). Using this large surface area without plating provides an array geometry favorable for neurotransmitter sensing, similar to traditional carbon fibers used for fast-scan cyclic voltammetry (Bucher & Wightman, 2015; Schwerdt, Kim, et al., 2017).

Novel, miniature, and implantable devices are required in order to further advance bioelectric medicines through the precise deciphering and monitoring of neural signals (Birmingham et al., 2014; Horn et al., 2019). The array presented here uses stable, biocompatible materials appropriate for clinical use, such as carbon fiber (Pusch & Wohlmann, 2018) and medical-grade elastomer. Metal coatings traditionally used in medical devices, such as platinum iridium or iridium oxide (Cassar et al., 2019; Lee, Hudak, Whalen, Petrossians, & Weiland, 2018; Petrossians, Whalen, Weiland, & Mansfeld, 2011), could replace the polymer electrode coating shown in this study to increase long-term stability. Although stimulation has not been explored by our group, coated carbon fiber electrodes have shown promising preliminary stimulation results in other studies (Gillis et al., 2017), which provides the prospect for further clinical uses of the array in the peripheral nervous system. Additionally, the promising architecture of this carbon fiber array may enable interfacing with difficult to access locations or small autonomic structures that require robust arrays for chronic implantation (Horn et al., 2019) in both current neuroscience studies and future medical applications.

There are, however, some difficulties for deploying these devices for large-scale use. The manual fabrication of the carbon fiber arrays is a time-intensive process that limits bulk manufacturing and requires an experienced fabrication technician. The application of silicone remains a challenging step limited by the small quantities needed to fill the aluminum mold wells and the small movements necessary to avoid placing the silicone on the fibers. To expand beyond four channels would likely require reorienting the polyimide backbone in the horizontal instead of vertical direction, requiring a new mold. While the blowtorching process can now be applied to whole arrays at once, replacing the individual lasering technique previously reported (Welle et al., 2020), it cannot currently be used to expose a pre-defined area of the carbon fibers. There is also still a need for a method of attachment to peripheral structures in chronic implants, such as suturing, Rose Bengal photochemical tissue bonding techniques (Yan et al., 2019), or silicone elastomer (Clark, Ledbetter, Warren, & Harrison, 2011). Future studies will need to investigate the chronic histological response of carbon fibers implanted in DRG and CVN.

Conclusion

Overall, this work examines novel mechanical improvements to carbon fiber electrode arrays for interfacing with the nervous systems and tests them in acute electrophysiology recording experiments. Sharpening the carbon fibers to lengths suitable for interfacing with small diameter rat nerves or deeper layers of the rat cortex greatly expands the use of carbon fibers electrodes. Sharpened carbon fibers can penetrate into stiff substrates, such as feline DRG and rat CVN, verifying that they have access to various recording targets despite their small diameter. The carbon fiber arrays embedded in silicone demonstrated robustness beneficial for *in vivo* surgical handling and chronic implantation in peripheral nervous system applications. We recorded acute electrophysiology from rat CVN, feline DRG, and rat motor cortex with sharpened carbon fibers. Our electrophysiology recordings from the DRG were the first reported recordings with carbon fiber electrode, to the best of our knowledge. The ease of insertion and robustness to movement make these arrays strong candidates for future chronic *in vivo* use.

Acknowledgements

We thank Dr. Stephen Kemp for experimental guidance, Dr. Lauren Zimmerman for initial surgical testing, Eric Kennedy for assistance in surgical preparation, David Ratze for experimental assistance and data analysis, and Hao Shen and Hope Thayer for fabrication assistance. The authors acknowledge the financial support of the University of Michigan College of Engineering and NSF grants #DMR-0320740 and #DMR-1625671, and thank the staff at the Michigan Center for Materials Characterization for their technical support. The authors thank the staff at the Lurie Nanofabrication Facility for their technical support. This research was supported by the National Institutes of Health

(NIH) Stimulating Peripheral Activity to Relieve Conditions (SPARC) Program (Award 1OT2OD024907) and National Science Foundation (Award 1707316).

Author Contributions

The study was planned by E.J.W., A.A.J., A.O., J.P.S., T.M.B., and C.A.C. Fabrication was done by E.J.W., J.E.W., J.M.R., and P.R.P. Surgeries and data collection were performed by E.J.W., A.A.J., E.C.B., A.O., and T.M.B. Benchtop testing and data collection were performed by E.J.W., J.E.W., and J.M.R. Data was analyzed by E.J.W., J.E.W., A.A.J., E.C.B., A.O., T.M.B., and C.A.C. The manuscript was drafted by E.J.W. and C.A.C. All authors reviewed and approved the final version of the manuscript.

References

Andersson, U., & Tracey, K. J. (2012). Neural reflexes in inflammation and immunity. *Journal of Experimental Medicine*, *209*(6), 1057–1068. https://doi.org/10.1084/jem.20120571

Badia, J., Boretius, T., Andreu, D., Azevedo-Coste, C., Stieglitz, T., & Navarro, X. (2011). Comparative analysis of transverse intrafascicular multichannel, longitudinal intrafascicular and multipolar cuff electrodes for the selective stimulation of nerve fascicles. *Journal of Neural Engineering*, *8*(3). https://doi.org/10.1088/1741-2560/8/3/036023

Bielefeldt, K., Zhong, F., Koerber, H. R., & Davis, B. M. (2006). Phenotypic characterization of gastric sensory neurons in mice. *American Journal of Physiology - Gastrointestinal and Liver Physiology*, *291*(5), 987–997. https://doi.org/10.1152/ajpgi.00080.2006

Birmingham, K., Gradinaru, V., Anikeeva, P., Grill, W. M., Pikov, V., McLaughlin, B., … Famm, K. (2014). Bioelectronic medicines: A research roadmap. *Nature Reviews Drug Discovery*, *13*(6), 399–400. https://doi.org/10.1038/nrd4351

Boretius, T., Badia, J., Pascual-Font, A., Schuettler, M., Navarro, X., Yoshida, K., & Stieglitz, T. (2010). A transverse intrafascicular multichannel electrode (TIME) to interface with the peripheral nerve. *Biosensors and Bioelectronics*, *26*(1), 62–69. https://doi.org/10.1016/j.bios.2010.05.010

Branner, A., & Normann, R. A. (2000). A multielectrode array for intrafascicular recording and stimulation in sciatic nerve of cats. *Brain Research Bulletin*, *51*(4), 293–306. https://doi.org/10.1016/S0361-9230(99)00231-2

Branner, A., Stein, R. B., Fernandez, E., Aoyagi, Y., & Normann, R. A. (2004). Long-Term Stimulation and Recording with a Penetrating Microelectrode Array in Cat Sciatic Nerve. *IEEE Transactions on Biomedical Engineering*, *51*(1), 146–157. https://doi.org/10.1109/TBME.2003.820321

Branner, A., Stein, R. B., & Normann, R. A. (2001). Selective Stimulation of Cat Sciatic Nerve Using an Array of Varying-Length Microelectrodes. *Journal of Neurophysiology*, *85*(4), 1585–1594.

Bucher, E. S., & Wightman, R. M. (2015). Electrochemical Analysis of Neurotransmitters. *Annual Review of Analytical Chemistry*, *8*, 239–261. https://doi.org/10.1146/annurev-anchem-071114-040426

Cassar, I. R., Yu, C., Sambangi, J., Lee, C. D., Whalen, J. J., Petrossians, A., & Grill, W. M. (2019). Electrodeposited platinum-iridium coating improves in vivo recording performance of chronically implanted microelectrode arrays. *Biomaterials*, *205*(November 2018), 120–132. https://doi.org/10.1016/j.biomaterials.2019.03.017

Charkhkar, H., Christie, B. P., Pinault, G. J., Tyler, D. J., & Triolo, R. J. (2019). A translational framework for peripheral nerve stimulating electrodes: Reviewing the journey from concept to clinic. *Journal of Neuroscience Methods*, *328*, 108414. https://doi.org/10.1016/j.jneumeth.2019.108414

Christensen, M. B., Pearce, S. M., Ledbetter, N. M., Warren, D. J., Clark, G. A., & Tresco, P. A. (2014). The foreign body response to the Utah Slant Electrode Array in the cat sciatic nerve. *Acta Biomaterialia*, *10*(11). https://doi.org/10.1016/j.actbio.2014.07.010

Clark, G. A., Ledbetter, N. M., Warren, D. J., & Harrison, R. R. (2011). Recording sensory and motor information from peripheral nerves with Utah Slanted Electrode Arrays. *Proceedings of the Annual International Conference of the IEEE Engineering in Medicine and Biology Society, EMBS*, 4641–4644. https://doi.org/10.1109/IEMBS.2011.6091149

Clerc, N., & Mei, N. (1983). Vagal Mechanoreceptors Located In The Lower Oesophageal Sphincter Of The Cat. *Journal of Physiology*, *336*, 487–498.

Davis, T. S., Wark, H. A. C., Hutchinson, D. T., Warren, D. J., O'Neill, K., Scheinblum, T., … Greger, B. (2016). Restoring motor control and sensory feedback in people with upper extremity amputations using arrays of 96 microelectrodes implanted in the median and ulnar nerves. *Journal of Neural Engineering*, *13*(3). https://doi.org/10.1088/1741-2560/13/3/036001

DeGiorgio, C., Heck, C., Bunch, S., Britton, J., Green, P., Lancman, M., … Soss, J. (2005). Vagus nerve stimulation for epilepsy: Randomized comparison of three stimulation paradigms. *Neurology*, *65*(2), 317–319. https://doi.org/10.1212/01.wnl.0000168899.11598.00

del Valle, J., & Navarro, X. (2013). *Interfaces with the peripheral nerve for the control of neuroprostheses*. *International Review of Neurobiology* (1st ed., Vol. 109). Elsevier Inc. https://doi.org/10.1016/B978-0-12-420045-6.00002-X

Deuschl, G., Schade-Brittinger, C., Krack, P., Volkmann, J., Schäfer, H., Bötzel, K., … Voges, J. (2006). A Randomized Trial of Deep-Brain Stimulation for Parkinson's Disease. *New England Journal of Medicine*, *355*(9), 896–908. https://doi.org/10.1056/nejmoa060281

El-Giar, E. E. D. M., & Wipf, D. O. (2006). Preparation of tip-protected poly(oxyphenylene) coated carbon-fiber ultramicroelectrodes. *Electroanalysis*, *18*(23), 2281–2289. https://doi.org/10.1002/elan.200603637

Famm, K., Litt, B., Tracey, K. J., Boyden, E. S., & Slaoui, M. (2013). A jump-start for electroceuticals. *Nature*, *496*, 159–161.

Fisher, L. E., Ayers, C. A., Ciollaro, M., Ventura, V., Weber, D. J., & Gaunt, R. A. (2014). Chronic recruitment of primary afferent neurons by microstimulation in the feline dorsal root ganglia. *Journal of Neural Engineering*, *11*(3). https://doi.org/10.1088/1741-2560/11/3/036007

Furniturewalla, A., Rustogi, P., Patrick, E., & Judy, J. W. (2019). Modeling the Recording of Intraneural Action Potentials with Microelectrodes Using FEM and Point-Source Methods. *International IEEE/EMBS Conference on Neural Engineering, NER*, 1191–1194. https://doi.org/10.1109/NER.2019.8717121

Gillis, W. F., Lissandrello, C. A., Shen, J., Pearre, B. W., Mertiri, A., Deku, F., … Gardner, T. J. (2017). Carbon fiber on polyimide ultra-microelectrodes. *Journal of Neural*

Engineering, *15*, 016010. https://doi.org/https://doi.org/10.1088/1361-6528/aa8b39

Green, R. A., Hassarati, R. T., Bouchinet, L., Lee, C. S., Cheong, G. L. M., Yu, J. F., … Lovell, N. H. (2012). Substrate dependent stability of conducting polymer coatings on medical electrodes. *Biomaterials*, *33*(25), 5875–5886. https://doi.org/10.1016/j.biomaterials.2012.05.017

Grill, W. M., Norman, S. E., & Bellamkonda, R. V. (2009). Implanted Neural Interfaces: Biochallenges and Engineered Solutions. *Annual Review of Biomedical Engineering*, *11*(1), 1–24. https://doi.org/10.1146/annurev-bioeng-061008-124927

Guitchounts, G., Markowitz, J. E., Liberti, W. A., & Gardner, T. J. (2013). A carbon-fiber electrode array for long-term neural recording. *Journal of Neural Engineering*, *10*(4), 046016. https://doi.org/10.1088/1741-2560/10/4/046016

Hong, G., Fu, T. M., Qiao, M., Viveros, R. D., Yang, X., Zhou, T., … Lieber, C. M. (2018). A method for single-neuron chronic recording from the retina in awake mice. *Science*, *360*(6396), 1447–1451. https://doi.org/10.1126/science.aas9160

Horn, C. C., Ardell, J. L., & Fisher, L. E. (2019). Electroceutical targeting of the autonomic nervous system. *Physiology*, *34*(2), 150–162. https://doi.org/10.1152/physiol.00030.2018

Janssen, D. A. W., Martens, F. M. J., de Wall, L. L., van Breda, H. M. K., & Heesakkers, J. P. F. A. (2017). Clinical utility of neurostimulation devices in the treatment of overactive bladder: Current perspectives. *Medical Devices: Evidence and Research*, *10*, 109–122. https://doi.org/10.2147/mder.s115678

Jiman, A. A., Ratze, D. C., Welle, E. J., Patel, P. R., Richie, J. M., Bottorff, E. C., … Bruns, T. M. (2020). Multi-channel intraneural vagus nerve recordings with a novel high-density carbon fiber microelectrode array. *Scientific Reports*, 1–13. https://doi.org/10.1101/2020.05.15.098301

Khani, H., & Wipf, D. O. (2019). Fabrication of Tip-Protected Polymer-Coated Carbon-Fiber Ultramicroelectrodes and pH Ultramicroelectrodes. *Journal of The Electrochemical Society*, *166*(8), B673–B679. https://doi.org/10.1149/2.0941908jes

Khurram, A., Ross, S. E., Sperry, Z. J., Ouyang, A., Stephan, C., Jiman, A. A., & Bruns, T. M. (2017). Chronic monitoring of lower urinary tract activity via a sacral dorsal root ganglia interface. *Journal of Neural Engineering*, *14*(3). https://doi.org/10.1088/1741-2552/aa6801

Kolarcik, C. L., Castro, C. A., Lesniak, A., Demetris, A. J., Fisher, L. E., Gaunt, R. A., … Cui, X. T. (2020). Host tissue response to floating microelectrode arrays chronically implanted in the feline spinal nerve. *Journal of Neural Engineering*, *17*(4). https://doi.org/10.1088/1741-2552/ab94d7

Kozai, T. D. Y., Langhals, N. B., Patel, P. R., Deng, X., Zhang, H., Smith, K. L., … Kipke, D. R. (2012). Ultrasmall implantable composite microelectrodes with bioactive surfaces for chronic neural interfaces. *Nature Materials*, *11*(12), 1065–1073. https://doi.org/10.1038/nmat3468

Lago, N., Yoshida, K., Koch, K. P., & Navarro, X. (2007). Assessment of biocompatibility of chronically implanted polyimide and platinum intrafascicular electrodes. *IEEE Transactions on Biomedical Engineering*, *54*(2), 281–290. https://doi.org/10.1109/TBME.2006.886617

Larson, C. E., & Meng, E. (2020). A review for the peripheral nerve interface designer. *Journal of Neuroscience Methods*, *332*, 108523. https://doi.org/10.1016/j.jneumeth.2019.108523

Lee, C. D., Hudak, E. M., Whalen, J. J., Petrossians, A., & Weiland, J. D. (2018). Low-Impedance, High Surface Area Pt-Ir Electrodeposited on Cochlear Implant Electrodes. *Journal of The Electrochemical Society*, *165*(12), G3015–G3017. https://doi.org/10.1149/2.0031812jes

Liu, J., Fu, T. M., Cheng, Z., Hong, G., Zhou, T., Jin, L., … Lieber, C. M. (2015). Syringe-injectable electronics. *Nature Nanotechnology*, *10*(7), 629–635. https://doi.org/10.1038/nnano.2015.115

Luan, L., Wei, X., Zhao, Z., Siegel, J. J., Potnis, O., Tuppen, C. A., … Xie, C. (2017). Ultraflexible nanoelectronic probes form reliable , glial scar – free neural integration. *Science Advances*, *3*, 1–10. https://doi.org/10.1126/sciadv.1601966

Lyttle, D. N., Gill, J. P., Shaw, K. M., Thomas, P. J., & Chiel, H. J. (2017). Robustness, flexibility, and sensitivity in a multifunctional motor control model. *Biological Cybernetics*, *111*(1), 25–47. https://doi.org/10.1007/s00422-016-0704-8

Marmerstein, J. T., McCallum, G. A., & Durand, D. M. (2021). Direct measurement of vagal tone in rats does not show correlation to HRV. *Scientific Reports*, *11*(1), 1–12. https://doi.org/10.1038/s41598-020-79808-8

McCallum, G. A., Sui, X., Qiu, C., Marmerstein, J., Zheng, Y., Eggers, T. E., … Durand, D. M. (2017). Chronic interfacing with the autonomic nervous system using carbon nanotube (CNT) yarn electrodes. *Scientific Reports*, *7*(1), 1–14. https://doi.org/10.1038/s41598-017-10639-w

Micera, S., Rossini, P. M., Rigosa, J., Citi, L., Carpaneto, J., Raspopovic, S., … Dario, P. (2011). Decoding of grasping information from neural signals recorded using peripheral intrafascicular interfaces. *Journal of NeuroEngineering and Rehabilitation*, *8*(1), 2–11. https://doi.org/10.1186/1743-0003-8-53

Moffitt, M. A., & McIntyre, C. C. (2005). Model-based analysis of cortical recording with silicon microelectrodes. *Clinical Neurophysiology*, *116*(9), 2240–2250. https://doi.org/10.1016/j.clinph.2005.05.018

Müller, H. H. O., Moeller, S., Lücke, C., Lam, A. P., Braun, N., & Philipsen, A. (2018). Vagus nerve stimulation (VNS) and other augmentation strategies for therapy-resistant depression (TRD): Review of the evidence and clinical advice for use. *Frontiers in Neuroscience*, *12*(239), 1–10. https://doi.org/10.3389/fnins.2018.00239

Navarro, X., Krueger, T. B., Lago, N., Micera, S., Stieglitz, T., & Dario, P. (2005). A Critical Review of Interfaces with the Peripheral Nervous System for the Control of Neuroprotheses and Hybrid Bionic Systems. *Journal of the Peripheral Nervous System*, *10*, 229–258. https://doi.org/10.1111/j.1085-9489.2005.10303.x

Nizampatnam, S., Saha, D., Chandak, R., & Raman, B. (2018). Dynamic contrast enhancement and flexible odor codes. *Nature Communications*, *9*(1). https://doi.org/10.1038/s41467-018-05533-6

Ntiloudi, D., Zanos, S., Gatzoulis, M. A., Karvounis, H., & Giannakoulas, G. (2019). How to evaluate patients with congenital heart disease-related pulmonary arterial hypertension. *Expert Review of Cardiovascular Therapy*, *17*(1), 11–18. https://doi.org/10.1080/14779072.2019.1550716

Obaid, A., Hanna, M. E., Wu, Y. W., Kollo, M., Racz, R., Angle, M. R., … Melosh, N. A. (2020). Massively Parallel Microwire Arrays Integrated with CMOS chips for Neural Recording. *Science Advances*, *6*. https://doi.org/10.1101/573295

Ostrowski, A. K., Sperry, Z. J., Kulik, G., & Bruns, T. M. (2017). Quantitative models of feline lumbosacral dorsal root ganglia

neuronal cell density. *Journal of Neuroscience Methods*, *290*, 116–124. https://doi.org/10.1016/j.jneumeth.2017.07.018

Otchy, T. M., Michas, C., Lee, B., Gopalan, K., Nerurkar, V., Gleick, J., … Gardner, T. J. (2020). Printable microscale interfaces for long-term peripheral nerve mapping and precision control. *Nature Communications*, *11*(1), 1–16. https://doi.org/10.1038/s41467-020-18032-4

Ouyang, Z., Sperry, Z. J., Barrera, N. D., & Bruns, T. M. (2019). Real-Time Bladder Pressure Estimation for Closed-Loop Control in a Detrusor Overactivity Model. *IEEE Transactions on Neural Systems and Rehabilitation Engineering*, *27*(6), 1209–1216. https://doi.org/10.1109/TNSRE.2019.2912374

Page, D. M., George, J. A., Kluger, D. T., Duncan, C., Wendelken, S., Davis, T., … Clark, G. A. (2018). Motor Control and Sensory Feedback Enhance Prosthesis Embodiment and Reduce Phantom Pain After Long-Term Hand Amputation. *Frontiers in Human Neuroscience*, *12*(352), 1–16. https://doi.org/10.3389/fnhum.2018.00352

Panda, B., Smiley, A., Majerus, S. J. A., Rietsch, A., Yang, J., Deng, K., … Bourbeau, D. J. (2020). SPARC: Wireless, Continuous Monitoring of Bowel State and Function. *Experimental Biology 2020 Meeting Abstracts*, *34*(S1).

Panebianco, M., Rigby, A., Weston, J., & Marson, A. G. (2015). Vagus nerve stimulation for partial seizures. *Cochrane Database of Systematic Reviews*, (4). https://doi.org/10.1002/14651858.CD002896.pub2

Patel, P. R., Na, K., Zhang, H., Kozai, T. D. Y., Kotov, N. A., Yoon, E., & Chestek, C. A. (2015). Insertion of linear 8.4 μ m diameter 16 channel carbon fiber electrode arrays for single unit recordings. *Journal of Neural Engineering*, *12*(4), 046009. https://doi.org/10.1088/1741-2560/12/4/046009

Patel, P. R., Popov, P., Caldwell, C. M., Welle, E. J., Egert, D., Pettibone, J. R., … Cai, D. (2020). High density carbon fiber arrays for chronic electrophysiology, fast scan cyclic voltammetry, and correlative anatomy. *Journal of Neural Engineering*, *17*(5). https://doi.org/10.1088/1741-2552/abb1f6

Patel, P. R., Zhang, H., Robbins, M. T., Nofar, J. B., Marshall, S. P., Kobylarek, M. J., … Chestek, C. A. (2016). Chronic in vivo stability assessment of carbon fiber microelectrode arrays. *Journal of Neural Engineering*, *13*, 066002. https://doi.org/10.1088/1741-2560/13/6/066002

Patil, A. C., & Thakor, N. V. (2016). Implantable neurotechnologies: a review of micro- and nanoelectrodes for neural recording. *Medical and Biological Engineering and Computing*, *54*(1), 23–44. https://doi.org/10.1007/s11517-015-1430-4

Paxinos, G., & Watson, C. (2007). *The Rat Brain in Stereotaxic Coordinates (New York: Academic)*. New York: Academic.

Petrossians, A., Whalen, J. J., Weiland, J. D., & Mansfeld, F. (2011). Electrodeposition and Characterization of Thin-Film Platinum-Iridium Alloys for Biological Interfaces. *Journal of The Electrochemical Society*, *158*, D269–D276. https://doi.org/10.1149/1.3578048

Pusch, J., & Wohlmann, B. (2018). Carbon Fibers. In *Inorganic and Composite Fibers* (pp. 31–51).

Saleh, M. S., Ritchie, S. M., Nicholas, M. A., Bezbaruah, R., Reddy, J. W., Chamanzar, M., … Panat, R. P. (2019). CMU Array: A 3D Nano-Printed, Customizable Ultra-High-Density Microelectrode Array Platform. *BioRxiv*, 1–29. https://doi.org/10.1101/742346

Schmidt, R. A., Jonas, U., Oleson, K. A., Janknegt, R. A., Hassouna, M. M., Siegel, S. W., & Van Kerrebroeck, P. E. V. (1999). Sacral nerve stimulation for treatment of refractory urinary urge incontinence. *Journal of Urology*, *162*(2), 352–357. https://doi.org/10.1016/S0022-5347(05)68558-8

Schwerdt, H. N., Kim, M. J., Amemori, S., Homma, D., Yoshida, T., Shimazu, H., … Cima, M. J. (2017). Subcellular probes for neurochemical recording from multiple brain sites. *Lab Chip*. https://doi.org/10.1039/C6LC01398H

Schwerdt, H. N., Shimazu, H., Amemori, K.-I., Amemori, S., Tierney, P. L., Gibson, D. J., … Graybiel, A. M. (2017). Long-term dopamine neurochemical monitoring in primates. *Proceedings of the National Academy of Sciences of the United States of America*, *114*(50), 13260–13265. https://doi.org/10.1073/pnas.1713756114

Settell, M. L., McConico, A. L., Nicolai, E. N., Knudsen, B. E., Shoffstall, A., Ross, E. K., … Ludwig, K. A. (2020). SPARC: A Road Map for Vagus Nerve Stimulation: Evidence of Vagotopy in a Swine Model. *Experimental Biology 2020 Meeting Abstracts*, *34*(S1).

Seymour, J. P., & Kipke, D. R. (2007). Neural probe design for reduced tissue encapsulation in CNS. *Biomaterials*, *28*(25), 3594–3607. https://doi.org/10.1016/j.biomaterials.2007.03.024

Siegel, S., Noblett, K., Mangel, J., Bennett, J., Griebling, T. L., Sutherland, S. E., … Berg, K. C. (2018). Five-Year Followup Results of a Prospective, Multicenter Study of Patients with Overactive Bladder Treated with Sacral Neuromodulation. *Journal of Urology*, *199*(1), 229–236. https://doi.org/10.1016/j.juro.2017.07.010

Skoglund, T. S., Pascher, R., & Berthold, C. H. (1997). The existence of a layer IV in the rat motor cortex. *Cerebral Cortex*, *7*(2), 178–180. https://doi.org/10.1093/cercor/7.2.178

Skousen, J. L., Merriam, S. M. E., Srivannavit, O., Perlin, G., Wise, K. D., & Tresco, P. A. (2011). Reducing surface area while maintaining implant penetrating profile lowers the brain foreign body response to chronically implanted planar silicon microelectrode arrays. In J. Schouenborg, M. Garwicz, & N. Danielsen (Eds.), *Progress in Brain Research* (Vol. 194, pp. 167–180). https://doi.org/10.1016/B978-0-444-53815-4.00009-1

Sperry, Z. J., Na, K., Parizi, S. S., Chiel, H. J., Seymour, J., Yoon, E., & Bruns, T. M. (2018). Flexible microelectrode array for interfacing with the surface of neural ganglia. *Journal of Neural Engineering*, *15*(3). https://doi.org/10.1088/1741-2552/aab55f

Straka, M. M., Shafer, B., Vasudevan, S., Welle, C., & Rieth, L. (2018). Characterizing longitudinal changes in the impedance spectra of in-vivo peripheral nerve electrodes. *Micromachines*, *9*(11), 1–21. https://doi.org/10.3390/mi9110587

Takmakov, P., Ruda, K., Phillips, K. S., Isayeva, I. S., Krauthamer, V., & Welle, C. G. (2015). Rapid evaluation of the durability of cortical neural implants using accelerated aging with reactive oxygen species. *Journal of Neural Engineering*, *12*(2), 1–16. https://doi.org/10.1088/1741-2560/12/2/026003

Tan, D. W., Schiefer, M. A., Keith, M. W., Anderson, J. R., Tyler, J., & Tyler, D. J. (2014). A neural interface provides long-term stable natural touch perception. *Science Translational Medicine*, *6*(257). https://doi.org/10.1126/scitranslmed.3008669

Wang, K., Frewin, C. L., Esrafilzadeh, D., Yu, C., Wang, C., Pancrazio, J. J., … Wallace, G. (2019). High-Performance Graphene-Fiber-Based Neural Recording Microelectrodes. *Advanced Materials*, *1805867*, 1–10.

https://doi.org/10.1002/adma.201805867
Wang, X., Hirschberg, A. W., Xu, H., Slingsby-Smith, Z., Lecomte, A., Scholten, K., … Meng, E. (2020). A Parylene Neural Probe Array for Multi-Region Deep Brain Recordings. *Journal of Microelectromechanical Systems*, *29*(4), 499–513. https://doi.org/10.1109/JMEMS.2020.3000235
Wark, H. A. C., Mathews, K. S., Normann, R. A., & Fernandez, E. (2014). Behavioral and cellular consequences of high-electrode count Utah Arrays chronically implanted in rat sciatic nerve. *Journal of Neural Engineering*, *11*(4). https://doi.org/10.1088/1741-2560/11/4/046027
Wark, H. A. C., Sharma, R., Mathews, K. S., Fernandez, E., Yoo, J., Christensen, B., … Tathireddy, P. (2013). A new high-density (25 electrodes/mm2) penetrating microelectrode array for recording and stimulating sub-millimeter neuroanatomical structures. *Journal of Neural Engineering*, *10*(4). https://doi.org/10.1088/1741-2560/10/4/045003
Welle, E. J., Patel, P. R., Woods, J. E., Petrossians, A., Della Valle, E., Vega-Medina, A., … Chestek, C. A. (2020). Ultra-small carbon fiber electrode recording site optimization and improved in vivo chronic recording yield. *Journal of Neural Engineering*, *17*(2). https://doi.org/10.1088/1741-2552/ab8343
Woods, J. E., Welle, E. J., Chen, L., Richie, J. M., Patel, P. R., & Chestek, C. A. (2020). Bending Properties of Materials for Peripheral Nerve Interfaces. *Proceedings of the 15th Annual IEEE International Conference on Nano/Micro Engineered and Molecular Systems*, 407–412. https://doi.org/10.1109/nems50311.2020.9265629
Yan, D., Jiman, A., Ratze, D., Huang, S., Parizi, S., Welle, E., … Seymour, J. (2019). Microneedle Penetrating Array with Axon-Sized Dimensions for Cuff-less Peripheral Nerve Interfacing. *International IEEE/EMBS Conference on Neural Engineering, NER*, *2019-March*, 827–830. https://doi.org/10.1109/NER.2019.8717097
Yoshida, K., Hennings, K., & Kammer, S. (2006). Acute performance of the thin-film longitudinal intra-fascicular electrode. *Proceedings of the First IEEE/RAS-EMBS International Conference on Biomedical Robotics and Biomechatronics*, 296–300. https://doi.org/10.1109/BIOROB.2006.1639102
Zanos, T. P., Silverman, H. A., Levy, T., Tsaava, T., Battinelli, E., Lorraine, P. W., … Bouton, C. E. (2018). Identification of cytokine-specific sensory neural signals by decoding murine vagus nerve activity. *Proceedings of the National Academy of Sciences of the United States of America*, *115*(21), E4843–E4852. https://doi.org/10.1073/pnas.1719083115